Research on Localization and Guidance for Space Rovers on Small Planetary Bodies

KyotoUniversity, Doctor Course Student
Graduate School of Engineering,
Department of Mechanical Engineering and Science
Sayaka KANATA

Tutor: Professor Tetsuo SAWARAGI

Abstract

Investigations into remote planetary bodies by robots are becoming increasingly important. Especially, investigations into small planetary bodies including asteroids and comets have gained considerable attention, because they are expected to have information about the birth and the growth of our solar system. Rovers are one of the most promising tools for direct investigations on remote planetary bodies, though, enormous uncertainties in environment make it difficult to guide such rovers. Conventional methods of localization cannot be applied to rovers on small planetary bodies because of uncertainties in the reference direction and strict limitations on on-board sensors. Since the rovers on small planetary bodies hop instead of crawl with wheels, they have large uncertainties in locomotion that conventional methods of control do not work.

The purpose of this research is to build a method to guide a robot on a small planetary body by a simple device. This paper mainly focuses on a method to localize a rover on small planetary body. The method is similar to the global positioning system in the point that it uses propagation delay of radio waves, though, the proposed method uses the round-trip distance between the mother spacecraft and the rover repeatedly. A single source of radio-waves is enough for the proposed method to work and no synchronization of clocks and no accurate clock on the rover is required. First, the proposed method has been formulated as a recursive method by applying Kalman filter to estimate the position of the rover in real-time. Numerical simulations assuming a rover was located on a small planetary body proved that the proposed method of localization can provide meter-order estimation even if the rover was located on a small planetary body of less than 1km in diameter. The simulation results also evaluated the influence of the ambiguities of the rotational motion of the small planetary body on localization accuracy: One degree of error in the direction of the rotational axis causes several meters error in the position of the rover.

Secondly, a method to estimate the rotational motion of the small planetary body together with the position of the rover has been proposed. The estimation problem has been formulated as an optimization problem to minimize a loss function, which has been defined based on the estimation errors derived in comparison with the actual measurements. Numerical simulations assuming a rover was located on a small planetary body

proved that normal gradient-based search do not work for this optimization problem. This was because the loss function has different scales of gradient value to each state variable. The minimum-search had to be divided into three steps depending on the scale of gradient value.

Thirdly, a method to solve the optimizatoin problem without calculation of differential has been introduced, which can be applied to any problem directly without calculation depending on the problem. In spite of calculating differentials, the proposed solution requires a large amount of computation to search the conjugate direction of the loss function. To reduce the amount of computation without loss of estimation accuracy, a method to select the measurement data so that the sensitivity directions of the selected data conserves has been reported. Numerical simulations assuming a rover was located on a small planetary body and experiments using a range measurement tool are shown to evaluate the estimation accuracy and computation time of the proposed method. These results have proved that the proposed solution for localization of a rover on small planetary body using round-trip measurement provide the optimal state as expected. The simulation results also proved that the proposed method to select the data can effectively reduce the computation time.

In addition to establishing a method to localize the rover on small planetary body, it is also important to build a system model to guide the hopping rover on a small planetary body. Roughness of the surface and varieties of conditions of contact between the rover and the surface of the small planetary body make it difficult to predict a hopping motion. Conventional methods to guide a rover such as velocity control and position control do not work for hopping rovers. Lastly in this paper, a model to guide a hopping rover is proposed, where the process of decision making is modeled as optimization process of multi-criteria problem, and the operator's preferences of the criteria are regarded as abstract objectives in control. The proposed system has been applied to a guidance problem of a hopping rover, and simulation results assuming a hopping rover was located on a small planetary body are reported to show the performance of the proposed model.

Acknowledgment

First and foremost I offer my sincerest gratitude to my supervisor, Professor Tetsuo Sawaragi, who always treated me as a researcher and gave me lots of chances to develop my skill as a researcher. His professional attitude to research such as considering things in broader view, large variety of interests and considerable stores of knowledge, affected me a lot.

I am heartily thankful to Dr. Hiroaki Nakanishi for his patience, motivation, enthusiasm, and immense knowledge. He continuously supported me on every activities as a researcher, and he enabled me to develop an understanding of the subject. His guidance helped me in all the time of Ph.D research from the preliminary to the concluding level.

I would like to express my sincere gratitude to Dr. Marek Makowski for continuous support on my research in Vienna. He taught me the importance of organizing documents and presentations and gave me lots of suggestions.

My sincere thanks also goes to Professor Ichiro Nakatani, who gave me hearty advice on my first journal even after I was graduated from his laboratory. I am deeply grateful to Dr. Tetsuo Yoshimitsu, who made me to complete my study in space robots at Tokyo University. His view as a space engineering researcher helped me to complete this thesis, too.

My warm thanks are due to our secretaries, Ms. Minato and Ms. Araki for supporting me by taking care of all the paperwork in the university and for cheered me by sweets and coffee. I wish to thank all staffs and members in Sawaragi laboratory. I felt the spirit of academic freedom from their common disposition; to respect each other's personality first of all.

I also thank Mr. Kido for suggesting me to study in Kyoto University and classmates in University of Tokyo. I am grateful to my colleges in Asahi-Kasei cooperation for their encouragement to study in University as a Ph.D student.

I take this opportunity to express my profound gratitude to my parent and parent in law for their moral support and patience during my study in Kyoto University. Finally, I offer my regards and blessings to my partner, Ryo, for his understanding, warm supprt and sincere encouragement.

Contents

Chapter 1

Introduction

Our solar system consists of a star, the Sun, the planets including Earth, Moon and Mars, numerous comets, asteroids, and meteoroids. The star and planets are relatively large that they have been thermally-metamorphosed. In contrast, small planetary bodies such as comets and asteroids do not have thermally-metamorphosed, or they are fragments of those have. Since these small planetary bodies are expected to have information about the birth and growth of the solar system, investigations into small planetary bodies attract several groups of scientists recent years.

Although several investigations into small planetary bodies have been realized, full-scale investigation was done by NEAR Shoemaker into the asteroid (433) Eros [1]. The Japanese Hayabusa probe started surveying asteroid Itokawa in 2005, and it succeeded in landing on and in taking off the surface of the asteroid [2]. The Hayabusa probe suggested that even an asteroid with approximately 500 m in diameter is covered with a variety of terrains [3,4]. For direct investigations into small planetary bodies, investigations by rovers are the most promising. The Hayabusa probe carried a robot Minerva, see Fig. 1.1, whose size is 0.1 m in diameter 0.12 m in height, and 0.6 kg in weight [5]. Because of micro gravity of asteroid Itokawa, a robot on the surface cannot move by wheels. The scientists developed MINERVA as a small hopping robot, which is specialized mechanism for locomotion under micro-gravity. Numerical simulations assumed a rover MINERVA on asteroid Itokawa have evaluated that a rover will hop 9 m distance taking 900 s with 0.05 m/s of initial hopping velocity [6]. To guide the rovers to destination points spread across a wide area, a method to localize the rover is required, which can 1) provide absolute positions of the rover in a planetary-body-centered frame, 2) cover the whole surface of the target planetary body. Moreover, it needs to be considered about 3) the size and mass of additional sensors on the rover, since there are strict limitations on on-board sensors due to the launch capability of the rocket carrying the rover.

The objective of this research is to build a method to guide a mobile robot to destination points under uncertainties. Rovers on small planetary bodies are focused on
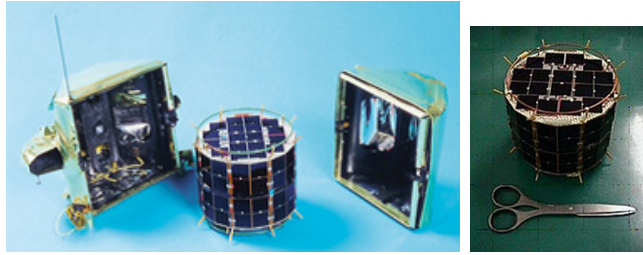
Fig. 1.1: Hopping robot, MINERVA. [7]

in this paper and methods to localize the rover and to estimate the environments are proposed considering strict limitations on on-board sensors. The proposed method is based on radio-waves and uses a mother spacecraft as a source of radio waves. In the proposed method of estimation, the measurements of round-trip propagation delay of radio waves, the information about the rotational motion of the small planetary body, and about the positions of the mother spacecraft are used. The proposed method is similar to Global Positioning System (GPS) in the point that it uses propagation delay of radio waves, though, only a single source of radio waves is enough in the proposed method: Measurements are done repeatedly to make pseudo-multiple reference points of radio sources. Moreover, no synchronization of clocks and no accurate clock is needed on the rover because the proposed method uses the measurements of round-trip propagation delay. The method is able to 1) provide absolute position of the rover in the planet-centered inertial frame, 2) cover the whole surface of the target planetary body, only requiring a transponder on the rover.

In chapter 2, a recursive method to localize the rover is proposed, which is based on Kalman filter. Wherein, it assumed that the rotational motion of the small planetary body to be precisely known. However, in many cases, it is difficult to estimate the rotational motion of a small planetary body. In chapter 3, a method to estimate the rotational motion of the small planetary body together with the position of the rover is introduced, which is formulated as an optimization problem to minimize the estimation error. In chapter 4, a method which do not require calculation of differentials is described, which can be applied directly to any problem. Simulation results are shown to evaluate the estimation accuracy of each method and also experimental results are reported, which support the feasibility of the proposed method.

Meanwhile, to guide the robot to destination point, an operator is necessary to cope with enormous uncertainties. To cope with these uncertainties, it is common to mount an autonomous system to select appropriate actions depending on the environment, however, the actions made by such autonomous systems may conflict with the operator's intention. These problems occur where multiple control-rules exist, and these rules are

independent even they have the same goal. It is necessary to design a system that consider such multiple rules explicitly. In chapter 5, a methodology to design a system for a control problem by two subjects, an operator and a robot, is described, which aims to provide dynamical and adaptive agreement in control. In general, operators have several criteria in control and these criteria conflict with each other, so the operators have to compromise a part of criteria in the process of decision making. The process of decision making is modeled as optimization process of multi-criteria problem. The operator's preferences of the criteria are regarded as abstract objectives in control in this paper. A methodology to design a system is proposed to provide agreement of the operator and the robot in control by sharing the preference balance between the operator and the robot. The proposed system is applied to a guidance problem of a space rover, and simulation results assuming a hopping rover is located on a small asteroid are reported to show the performance of the proposed system. Chapter 6 concludes this paper.

Chapter 2

Radio Wave Based Localization of a Rover for a Small Planetary Body

2.1 Introduction

Since conventional rovers on lunar and Mars investigated in the vicinity of the lander [8–10], it was sufficient to localize the rover relative to the lander. In contrast, rovers on small planetary bodies are expected to investigate wide area relative to the size of the target planetary body, so, relative localization using a lander is useless. To guide the rover to destination points spread across a wide area, a method to localize a rover has to 1) provide absolute positions of the rover in a planetary-body-centered frame, 2) cover the whole surface of the target planetary body. In addition, localization accuracy required for rovers on small planetary bodies is meter-order, because one kind of the most interesting points to be studied is an artificial crater, which have at most several meters in radius. Moreover, 3) the size and mass of additional sensors on the rover must be considered since there are strict limitations on on-board sensors due to the launch capability of the rocket carrying the rover. Real-time localization is preferable to guide the rover dynamically.

In this chapter, a method of localization is proposed, which satisfies the above requirements. The applicability of the conventional methods of localization is discussed in section 2.2. In section 2.3, a method of localization using the round-trip propagation delay of radio waves between the rover and the mother spacecraft is presented. In order to estimate the rover in real-time, recursive method using Kalman filter [11] is described. In section 2.4, simulation results to evaluate the estimation accuracy of the proposed method are shown, which assumed a rover is located on the surface of a small planetary body of 600 m in diameter. Influence analysis on localization accuracy of the rover of uncertainties in the rotational parameters and positions of the mother spacecraft is summarized in 2.5. A recursive method to reduce the influence on localization accuracy is

15

described in section 2.6. Section 2.7 summarizes this chapter.

2.2 Problems in Applying Conventional Methods

In this section, problems in applying conventional methods of localization to rovers on small planetary bodies of less than 1000 m in diameter are summarized.

2.2.1 Localization using Image Matching

The idea of matching global and local information [1], such as images [12], scanned information [13–17], are attractive in the points that they provide localization without modification of the environment and without external resources. For space rovers, global maps need to be made by orbiters [15, 16]. Since rovers are expected to move widely on the surface of the small planetary body, global maps that cover the whole surface is required. On the other hand, the range of the local information depends on the rover's height. For example, a rover MINERVA's height and its diameter were 0.1 m and 0.12 m, respectively [5], which had been carried on Hayabusa probe [3, 18]. Thus, a rover on a small planetary body is tiny, in general, and the range of view of the rover is too small to match the resolution of the global data collected by the spacecraft.

Yan et. al. proposed a method to determine the position and attitude of a hopping rover in real time using optical flows of the terrain obtained during the hopping motion [19]. Since it estimates the position and attitude in a planetary-body fixed surface frame, it is necessary to transform these estimations into a planetary-body-centered inertial frame.

In case that the global data is not available, or not reliable, simultaneous localization and mapping is needed [20]. However, a rover on a small planetary body requires strict limitation to mass and volume of instruments on board. It also has a problem in the range of view of the rover.

2.2.2 Localization Observing Stars and Sun

Celestial navigation [21] also realizes localization without external resources and without environment modification. As star trackers are high-cost and heavy, a method using CCD sensors to observe celestial vectors of Sun and Earth [22] is feasible.

To determine the celestial direction of the sun and the stars, reference directions is required. As illustrated in Fig.2.1, the observer on the surface on the target body measures the direction of stars in the geodetic coordinate system, which refers the direction of gravitational force. On the other hand, in a inertial coordinate frame, the direction of geocentric coordinate system is taken, which referees the rotational axis as a reference

direction [23,24] Earth is large and almost sphere that the gravitational force measured on the surface pass through the center of mass. In contrast, the gravitational force measured on the surface of the small planetary body does not always pass through the center of mass because of the irregular shape and micro gravity [25]. The direction error causes crucial effect on the localization accuracy.

2.2.3 Localization by Radio-Waves

The position of the rover can also be determined from measurements based on radio systems. In Mars Exploration Rover mission, measurement of round-trip Doppler shift using ultra high frequency of radio waves was expected to localize a rover with the accuracy of 1 to 10 m in the Mars inertial system [16]. For a rover on a small planetary body, since relative velocity of the orbiter to the rover is limited because of the micro gravity of the small planetary body, Doppler shift between the rover and an orbiter will be too small to detect.

GPS is widely used on Earth, which uses one-way propagation delay of radio waves from GPS satellites to a receiver. Multiplying light speed by measured propagation delay provides pseudo-distance between the receiver and the GPS satellite, which are collected from at least 3 satellites as illustrated in Fig.2.2. Thus, it requires multiple satellites as radio sources [26,27] and clock synchronization is required between the receiver and GPS satellites for accurate localization. It is not feasible to arrange multiple satellites near small planetary body and to load precise clock on the rover on small planetary body.

Navigation based on range measurements is still attractive, because communication device can be used for localization. Moreover, there is no atmospheric delay on the small planetary body, which is the main cause of estimation error in GPS, so, the accuracy of the range measurement on small planetary body will be high enough. If a method of localization requiring only a single source of radio-waves is achieved, it will provide accurate localization even for the rovers on small planetary bodies.

2.3 Localization Method using Round-trip Propagation Delay

2.3.1 Assumptions

A method to localize a rover based on radio waves is illustrated in Figure 2.3: A mother spacecraft near a small planetary body transmits a radio signal and a rover on the surface of the small planetary body reflects it and the spacecraft receives the reflected signal again. The measurement of round-trip propagation delay between the mother spacecraft and the rover is conducted repeatedly. The mother spacecraft estimates the
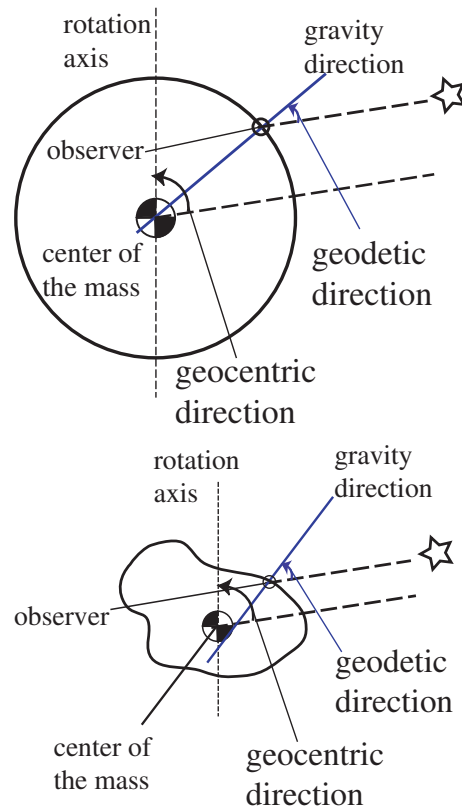
Fig. 2.1: Geocentric and geodetic direction on Earth (left) and
on a small planetary body (right) : The geocentric direction uses
rotation axis as a reference direction and the geodetic direction uses
gravity direction as a reference. On Earth, the gravity direction
and the rotation axis crosses at the center of the mass. On a small
planetary body, the gravity direction measured on the surface does
not always pass through the center of the mass.

rover's position by the measurement data and sends the processed information to the
rover.

- Assumption 1: The rover does not move during the measurement.

  The rover remains stationary on the surface of the small planetary body during
  the measurement. The rover's motion only depends on the rotational motion of
  the small planetary body.

  The rover's task is not only to locomote. There are other important tasks such as
  scientific observation and data transmission. During the night, the rover cannot
  charge the battery to save the power, so, it should not move around. Thus, this
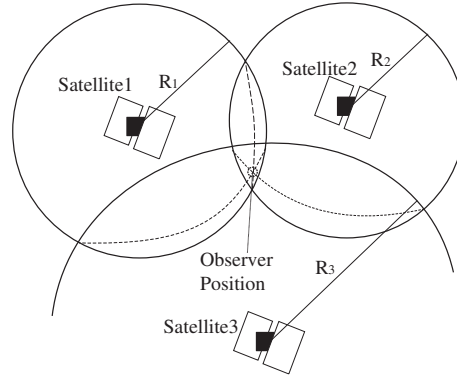
Fig. 2.2: Image of GPS method : this method needs several satellites (at least three) to determine the position of the observer.
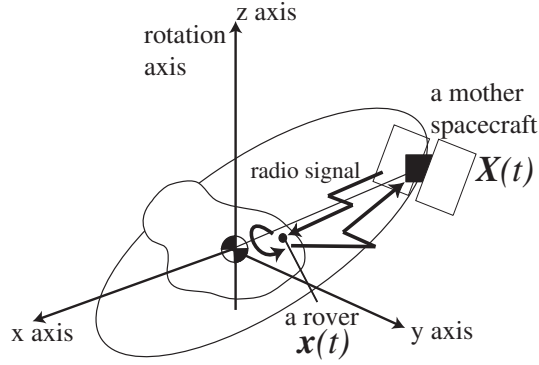
Fig. 2.3: Definition of coordinates for proposed method

assumption is reasonable.

- Assumption 2: The rotational parameters of the small planetary body are precisely known. The center of mass, the rotational period and the direction of the rotational axis are assumed to be precisely known.

  Normally, the mother spacecraft investigates the target planetary body prior to the investigations by the rover and makes terrain maps, gravity maps and estimates the direction of the rotational axis of the target planetary body [28, 29].

- Assumption 3: The mother spacecraft orbits around the small planetary body and the orbit parameters of the mother spacecraft are known.

  The positions of the spacecraft is determined by referring the direction of the sun, arrangement of the stars and specific terrain of the planetary body surface [30]. The orbit parameters are derived from these positions.

- Assumption 4: Processing delay on a transponder on the rover is statistically known.

  To identify the reflected radio waves of the rover from the reflection from the surface of the small planetary body, a transponder is assumed to be loaded on the rover.

2.3.2 Coordinate Definition

The inertial-fixed coordinate frame as illustrated in Fig. 2.3 is used. Its origin is fixed to the center of mass of the small planetary body. Define z axis is parallel to the nominal direction of the rotation axis of the small planetary body. The x axis coincides with the longitude of the ascending node of the spacecraft's orbit. The y axis is defined to be perpendicular to x and z axes and that the coordinate system is a right-handed system. $\boldsymbol{X}$ denotes the position of the spacecraft and $\boldsymbol{x} = [x, y, z]^T$ denotes the position of the rover, where ^{T} means transpose of matrix. $\boldsymbol{\sigma} = [\sigma_x, \sigma_y, \sigma_z]^T$ and ω denote the direction of the rotation axis and the angular velocity of the small planetary body, respectively.

2.3.3 Equation of State Prediction

From Assumption 1, the motion of the rover depends only on the rotational motion of the small planetary body. From Assumption 2, the motion of the small planetary body is precisely known that the state prediction of the rover is expressed as

$$\boldsymbol{x}(t) = \boldsymbol{R}_z\left(\omega(t - t_0)\right)\boldsymbol{x}(t_0), \tag{2.1}$$

where ω is the angular velocity of the rotational motion of the small planetary body, $\boldsymbol{R}_z$ is the rotation matrix of z axis. From the assumption 3, the positions of the mother spacecraft are described using six orbit parameters. Ψ_l : longitude of the ascending node, Ψ_I : the inclination, Ψ_A : the semi major axis, Ψ_ε : the eccentricity, Ψ_ω : the argument of perigee and Ψ_{M_0} : the mean anomaly at t_0 [28]. Using the mean motion $\Psi_n = (Gm/\Psi_A^3)^{1/2}$, the mean anomaly is given by $\Psi_{M_t} = \Psi_n(t - t_0) + \Psi_{M_0}$, where G is universal gravity constant and m is the mass of the small planetary body. From Kepler Equation (2.2), we can numerically acquire eccentric anomaly Ψ_{E_t}.

$$\Psi_{M_t} = \Psi_{E_t} - \Psi_\varepsilon \sin \Psi_{E_t} \tag{2.2}$$

The position of the mother spacecraft on the orbit plane is given by

$$\begin{bmatrix} X_{obt}(t) \\ Y_{obt}(t) \\ Z_{obt}(t) \end{bmatrix} = \begin{bmatrix} \Psi_A(\cos \Psi_{E_t} - \Psi_\varepsilon) \\ \Psi_A\sqrt{1 - \Psi_\varepsilon^2}\sin \Psi_{E_t} \\ 0 \end{bmatrix} \tag{2.3}$$

Transforming $\boldsymbol{X}_{obt}(t)$ into the inertial fixed coordinate system, the position of the mother spacecraft $\boldsymbol{X}(t)$ is described by

$$\begin{bmatrix} X(t) \\ Y(t) \\ Z(t) \end{bmatrix} = \boldsymbol{R_z}(-\Psi_l)\boldsymbol{R_x}(-\Psi_I)\boldsymbol{R_z}(-\Psi_\omega) \begin{bmatrix} X_{obt}(t) \\ Y_{obt}(t) \\ Z_{obt}(t) \end{bmatrix} \tag{2.4}$$

where $\boldsymbol{R_x}$ denotes the rotation matrix of the x axis.

2.3.4 Measurement Equation

As illustrated in Fig. 2.4, the measurement, τ_{ob}, satisfies eq.(2.5) geometrically.

$$\tau_{ob} = \frac{1}{c}\left(\|\boldsymbol{X}(t_e) - \boldsymbol{x}(t_{ref})\| + \|\boldsymbol{X}(t_r) - \boldsymbol{x}(t_{ref})\|\right) + \eta, \tag{2.5}$$

where c denotes light speed, η denotes the measurement noise, t_e is the transmission time, t_r is the receiving time at the mother spacecraft, and t_{ref} is the reflection time at the rover. For the further discussion, define

$$g(\boldsymbol{x}(t_e)) = \frac{1}{c}\left(\|\boldsymbol{X}(t_e) - \boldsymbol{x}(t_{ref})\| + \|\boldsymbol{X}(t_r) - \boldsymbol{x}(t_{ref})\|\right). \tag{2.6}$$

From Assumption 4, the average and variance of the measurement noise, η, are known.

$$E[\eta] = 0, \tag{2.7}$$
$$E[\eta^2] = \gamma^2, \tag{2.8}$$

where the function $E[x]$ denotes the average of x. The position of the mother spacecraft at reception time, $\boldsymbol{X}(t_r)$, is calculated by the position of the spacecraft at emission time, $\boldsymbol{X}(t_e)$, using orbit parameters. The position of the rover, $\boldsymbol{x}(t_e)$, the measurement, $\tau = ob$, are described by the position of the rover at emission, $\boldsymbol{x}(t_e)$. $\tau = ob$ can be divided in two terms, τ_d (downward : from the mother spacecraft to the rover) and τ_u (upward : from the rover to the mother spacecraft), as below :

$$\tau_d = \frac{1}{c}\|\boldsymbol{X}(t_e) - \boldsymbol{x}(t_{ref})\| \tag{2.9}$$

$$\tau_u = \frac{1}{c}\|\boldsymbol{X}(t_r) - \boldsymbol{x}(t_{ref})\|. \tag{2.10}$$

2.3.5 Real-time Maximum Likelihood Estimation

Assume that the measurement are conducted every ΔT. To estimate the position of the rover in real-time, extended Kalman Filter has been applied [11, 31–33] since the
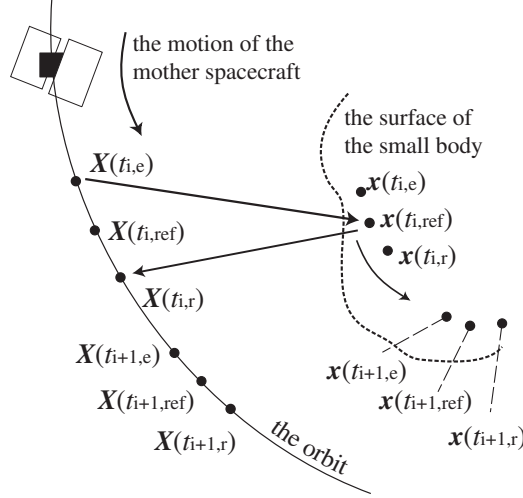
Fig. 2.4: Two-way range measurement of proposed method

observation equation is nonlinear. The position of the rover, $\boldsymbol{x}(t_e)$, at emission time of radio waves, t_e, is estimated recursively. The i-th measurement is

$$\boldsymbol{\tau}_{ob,i} = g(\boldsymbol{x}^*(t_{e,i})) + \eta_i, \tag{2.11}$$

where the suffix i indicates i-th observation at $(t_0 + i\Delta T)$, and * denotes actual value. Define $\boldsymbol{x}(i|j)$ as the predicted state of the rover's position at time i using information at time j, where it means estimation in case of $i = j$. The measurement update and time update and are expressed by using the covariance matrix of estimation error, $\boldsymbol{P}$, as follows

$$\hat{\boldsymbol{x}}(i|i) = \hat{\boldsymbol{x}}(i|i-1) + \boldsymbol{K}(i)\left[\tau_{ob}(i) - g\left(\hat{\boldsymbol{x}}(i|i-1)\right)\right], \tag{2.12}$$

$$\boldsymbol{P}(i|i) = \boldsymbol{P}(i|i-1) - \boldsymbol{K}(i)\boldsymbol{L}(i)\boldsymbol{P}(i|i-1), \tag{2.13}$$

$$\hat{\boldsymbol{x}}(i+1|i) = \Phi\hat{\boldsymbol{x}}(i|i) + \boldsymbol{w}(i), \tag{2.14}$$

$$\boldsymbol{P}(i+1|i) = \Phi\boldsymbol{P}(i|i)\Phi^T + \boldsymbol{Q}(i), \tag{2.15}$$

where ˆ denotes the estimated value and

$$\boldsymbol{K}(i) = \boldsymbol{P}(i|i-1)\boldsymbol{L}(i)^T\left[\boldsymbol{L}(i)\boldsymbol{P}(i|i-1)\boldsymbol{L}(i)^T + r(i)\right]^{-1}, \tag{2.16}$$

$$\boldsymbol{Q}(i) = E\left[\left(\boldsymbol{w}(i) - E\left[\boldsymbol{w}(i)\right]\right)\left(\boldsymbol{w}(i) - E\left[\boldsymbol{w}(i)\right]\right)^T\right]. \tag{2.17}$$

$\boldsymbol{w}$ denotes propagation noise, and $\boldsymbol{L}$ is defined as

$$\boldsymbol{L} = \left\{\frac{\partial g}{\partial \boldsymbol{x}(t_e)}\right\} \tag{2.18}$$

and the size of $\boldsymbol{L}$ is 1×3. Φ in eq. (2.15), eq.(2.14) denotes the motion of the rover $\boldsymbol{x}$ that $\Phi = \boldsymbol{R}_z(\omega \Delta t)$.

Estimation of Measurement Value τ_{ob} :

The measurement value, $\tau(i+1|i)$, is divided into two values $\tau_d(i+1|i)$ and $\tau_u(i+1|i)$. They are calculated from the estimated state at i-th measurement, $\hat{\boldsymbol{x}}(i|i-1)$. $\hat{\tau}_d$ is given by solving

$$c\hat{\tau}_d = \|\boldsymbol{X}_e - \boldsymbol{R}_z(\hat{\tau}_d)\boldsymbol{x}_e\|, \tag{2.19}$$

where $\boldsymbol{X}_e = \boldsymbol{X}(t_{e,i})$ and $\boldsymbol{x}_e = \hat{\boldsymbol{x}}(i|i-1)$. It is necessary to solve eq.(2.19) numerically. In the following, all the value represents i-th measurement that the suffix i is omitted. Using $\hat{\tau}_d$, the propagation delay of $\hat{\tau}_u$ can be given by solving

$$c\hat{\tau}_u = \|\boldsymbol{X}(t_e + \hat{\tau}_d + \hat{\tau}_u) - \boldsymbol{R}_z(\hat{\tau}_d)\boldsymbol{x}_e\|. \tag{2.20}$$

It is necessary to solve Kepler's equation (2.2) to determine $\boldsymbol{X}(t_e + \tau_d + \hat{\tau}_u)$. We can solve eq. (2.20) by a method of successive approximation.

Deviation of Measurement Value and Position of the Rover :

$\boldsymbol{L}$ in eq. (2.13) is deviation of τ depending on the position of the rover at emission of radio waves, $\boldsymbol{x}(t_e)$.

$$\boldsymbol{L} = \partial g / \partial \boldsymbol{x}_e \tag{2.21}$$
$$= \partial \tau_d / \partial \boldsymbol{x}_e + \partial \tau_u / \partial \boldsymbol{x}_e \tag{2.22}$$

From eq. (2.19) and (2.20),

$$\frac{\partial \tau_d}{\partial \boldsymbol{x}_e} = \frac{1}{\Psi_{A,\tau_d}} \left(\boldsymbol{x}_e - \boldsymbol{R}_z(-\omega \tau_d)\boldsymbol{X}_e \right)^T \tag{2.23}$$

$$\frac{\partial \tau_u}{\partial \boldsymbol{x}_e} = \frac{1}{\Psi_{A,\tau_u}} \left(\boldsymbol{X}_r - \boldsymbol{x}_{ref} \right)^T \left(\frac{d\boldsymbol{X}_r}{dt} \cdot \frac{\partial \tau_d}{\partial \boldsymbol{x}_e} - \frac{\partial \boldsymbol{x}_{ref}}{\partial \boldsymbol{x}_e} \right) \tag{2.24}$$

where $\boldsymbol{X}(t_r) = \boldsymbol{X}_r \quad \boldsymbol{x}(t_{ref}) = \boldsymbol{x}_{ref}$.

$$\Psi_{A,\tau_d} = c^2 \tau_d + (X_e x_e + Y_e y_e)\omega \sin(\omega \tau_d) + (X_e y_e - Y_e x_e)\omega \cos(\omega \tau_d) \tag{2.25}$$

$$\Psi_{A,\tau_u} = c^2 \tau_u - (\boldsymbol{X}_r - \boldsymbol{x}_{ref})^T \frac{\partial \boldsymbol{X}_r}{\partial \tau} \tag{2.26}$$

$$\frac{\partial \boldsymbol{X}_r}{\partial \tau} = \boldsymbol{R}_z(-\Psi_\Omega)\boldsymbol{R}_x(-\Psi_\theta)\boldsymbol{R}_z(-\Psi_\omega)\frac{d\boldsymbol{X}_{obt}}{dt} \tag{2.27}$$

$$\frac{\partial \boldsymbol{X}_{obt}}{\partial \tau} = \begin{bmatrix} \Psi_A(-\sin \Psi_{Et})\frac{\partial \Psi_{Et}}{\partial \tau} \\ \Psi_A \sqrt{1 - \Psi_\varepsilon^2} \cos \Psi_{Et} \frac{\partial \Psi_{Et}}{\partial \tau} \\ 0 \end{bmatrix} \tag{2.28}$$

$$\frac{\partial \Psi_{Et}}{\partial \tau} = \frac{\Psi_n}{1 - \Psi_\varepsilon \cos \Psi_{Et}(\tau)} \tag{2.29}$$

$$\frac{\partial \boldsymbol{x}_{ref}}{\partial \boldsymbol{x}_e} = \boldsymbol{R}_z(\omega \tau_d) + \frac{\partial \tau_d}{\partial \boldsymbol{x}_e} \begin{bmatrix} -x_e \omega \sin(\omega \tau_d) + y_e \omega \cos(\omega \tau_d) \\ -x_e \omega \cos(\omega \tau_d) - y_e \omega \sin(\omega \tau_d) \\ 0 \end{bmatrix}^T \tag{2.30}$$

$\hat{\boldsymbol{x}}_{ref}$ and $\hat{\boldsymbol{X}}_r$ are calculated from the estimated values of propagation delay, $\hat{\tau}_d$ and $\hat{\tau}_u$, where $\hat{\boldsymbol{x}}_{ref} = \boldsymbol{x}(t_e + \hat{\tau}_d)$ $\hat{\boldsymbol{X}}_r = \boldsymbol{X}(t_e + \hat{\tau}_d + \hat{\tau}_u)$.

2.3.6   Method to Reduce Amount of Calculation

Since the less amount of calculation is the more preferable even for the computers on mother spacecraft, a method to reduce the amount of calculation required on the mother spacecraft is proposed.

The proposed method of localization described in the above subsection, both the propagation delay of down-ward delay, τ_d, and up-ward delay, τ_u, has to be calculated. It requires to solve the Kepler's equation, which cannot be solved analytically that requires large amount of calculation. By using the actual position, $\boldsymbol{X}_{r,ob}$, instead of calculating the position of the mother spacecraft at reception time, $\hat{\boldsymbol{X}}_r$, it can reduce the amount of calculation to almost half, since there is no need to calculate the down-ward propagation time of up-ward. That is, estimate $\hat{\tau}_d$ from eq. (2.19) as

$$\tau_{ob} - \hat{\tau}_d = \frac{1}{c}\|\boldsymbol{X}(t_{r,ob}) - \boldsymbol{R}_z(\hat{\tau}_d)\boldsymbol{x}_e\|. \tag{2.31}$$

2.4   Evaluation by Numerical Simulations

2.4.1   Simulation Parameters

We assumed a rover was located on a surface of a spheroid planetary body of 600 m in diameter referring asteroid Itokawa [34]. Parameters of the small planetary body, the nominal state and the orbit parameters of the mother spacecraft are summarized in Table 2.1. The measurement noise was assumed as white Gaussian with variance 10^{-16} s^2, which reflected the performance of a recent transponder for space use. The initial error in estimation of the rover's position was assumed to be 10 m in each direction, which was approximately 20 m in total. Since the rotational motion of the small planetary body was assumed to be precisely known, the covariance matrix of estimation error, $\boldsymbol{Q}$ was set to $\boldsymbol{0}$. The range of view of the rover was assumed to be 80 deg from zenith, and

Table 2.1: Simulation parameters

rover	visibility	80 deg from zenith
planetary body	size (diameter)	300×300×600 m
	density	2500 kg/m^3
nominal state	rover's position $\bar{\boldsymbol{x}}$	$[0, 300, -100]^T$ m
	rotation axis, $\bar{\boldsymbol{\sigma}}$	$[0, 0, 1]^T$
	angular vel., $\bar{\omega}$	1.4×10^{-4} rad/s
spacecraft orbit	long. of asc. node	0 rad
	inclination	1 rad
	semi-major axis	3000 m
	eccentricity	0.2
	arg.,of perigee	0 rad
	mean anomaly at epoch	0 rad

the measurement data when the rover could catch the mother spacecraft in sight was collected. The interval of measurement, ΔT, was 60 s.

2.4.2 Evaluation of Estimation Accuracy

Simulation results processed by extended Kalman Filter are plotted in Figure 2.5. The results were calculated through Monte Carlo analysis, where 100 particles were used. The horizontal axis denotes elapsed time after the observation started and the vertical axis denotes the average error in estimation, $\|\Delta \boldsymbol{x}\| = \|\boldsymbol{x}^* - \hat{\boldsymbol{x}}\|$, of 100 particles.

Fig.2.5 suggests that the rover can be localized with the accuracy of 1 m by 4 hours observation. During the 4 hours observation, the position of the rover was 600 m away from the initial position, while the position of the mother spacecraft was 500 m away to the opposite direction to the rover's motion, therefore, variation in relative position was approximately 1000 m. Fig.2.5 suggests that the estimation error decreased in accordance with the increase in the observation time, which proves that the proposed method of estimation can provide the actual state as expected.

In Fig.2.6, the diagonal components of the covariance matrix $\boldsymbol{P}$ are plotted. This indicates that firstly x element was determined, next was y and lastly the z element settled. The variance in estimation error decreased in accordance with the observation time, which supports the convergence of the proposed method of estimation.

As the proposed method of estimation uses the measurements of round-trip propagation delay between the mother spacecraft and the rover, it has sensitivity in line-of-sight direction. The relative position of the rover and the mother spacecraft explains the trend
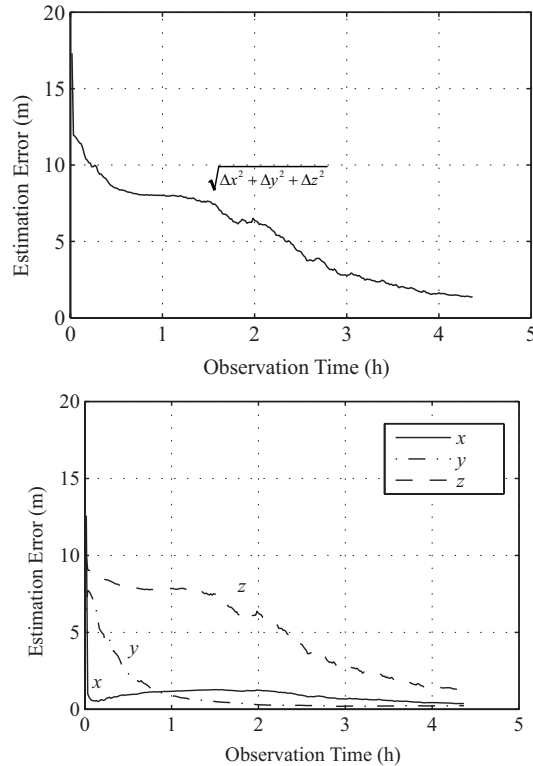
Fig. 2.5: Dependency of estimation error in position and observation time : While x and y element errors are correctly determined fast, the z element error remains. (above) total error (below) error along each direction

of estimation error in each component. The relative positions between the rover and the mother spacecraft in accordance with the observation time are plotted in Fig. 2.7. The line-of-sight direction was almost parallel to x-axis direction, which is perpendicular to the worst estimation in z direction. Since z-axis was defined to be parallel to the direction of the rotational axis, z element represents the latitude of the rover's position. Latitude is constant during the rotational motion of the small planetary body. Thus, only the orbital motion of the mother spacecraft contributes to provide the sensitivity in the direction of z-axis. For small planetary bodies like asteroid Itokawa, the gravitational force is so small that rotational motion of the small planetary body provides much larger variation to the sensitive directions than the motion of the spacecraft orbiting around the small planetary body. Therefore, estimation error in x-axis direction reduced first, then error in y-axis direction reduced by the rotational motion of the small planetary body, then error in z-axis reduced in the end. If the mother spacecraft was arranged around
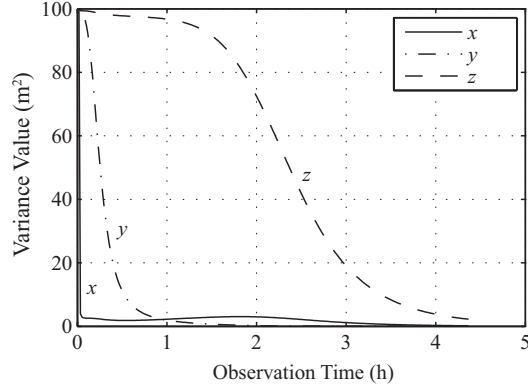
26

Fig. 2.6: Variance of each element and observation time : Firstly the variance of x is minimized, the second is y element, and finally z element reduced.

the pole region of the small planetary body, it will provide more accurate estimation in z element. Numerical analysis on sensitivity direction is given in chapter 3.

2.4.3 Evaluation of Method to Reduce Calculation Amount

The method to reduce the amount of calculation, was evaluated. The estimation results are plotted in Fig. 2.8, where the simulation parameters were the same with the results plotted in Fig. 2.5. Even the method cut almost half process in estimation, the results are as accurate as the results from the original method of estimation. This suggests that the estimated position of the spacecraft at reception time, $\hat{\boldsymbol{X}}_r$, and the measured position, $\boldsymbol{X}_{r,ob}$ satisfy $\hat{\boldsymbol{X}}_r \sim \boldsymbol{X}_{r,ob}$ and the difference between them is ignorable. In this chapter, the motion of the mother spacecraft was assumed to be precisely known. Since the motion of the mother spacecraft was given by six orbit parameters, $\hat{\boldsymbol{X}}_r$ and $\boldsymbol{X}_{r,ob}$ exist in the same orbit. The longitude of ascending node Ψ_l, was 3000 m and the period of the orbit was 130 h while the propagation delay, τ, was approximately 2×10^{-5} s. Wherein, the position difference between $\boldsymbol{X}_e$ and $\boldsymbol{X}_r$ is given by $2\pi l \tilde{\tau}/T$, it is 10^{-6} m, which is sufficiently small than the distance between the rover and the mother spacecraft. As the difference between $\hat{\boldsymbol{X}}_r$ and $\boldsymbol{X}_{r,ob}$ is much smaller than that of $\boldsymbol{X}_e$ and $\boldsymbol{X}_r$, using the measured value, $\boldsymbol{X}_{r,ob}$, instead of estimating $\hat{\boldsymbol{X}}_r$ provided as accurate estimation as the original method.
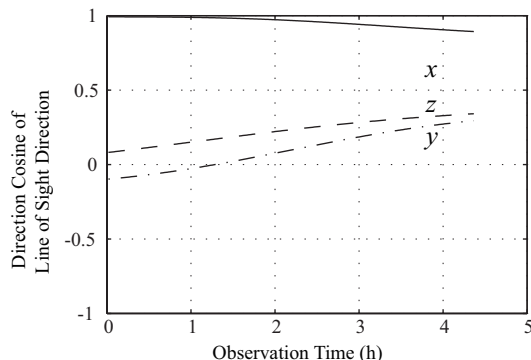
Fig. 2.7: Line-of-sight directions from rover to mother spacecraft

2.4.4 Summary of Simulation Results

Numerical simulations assuming a rover on the asteroid Itokawa proved that the proposed method of localization provides sufficiently accurate estimation of the position of the rover; after 4 hours of observation, estimation error was 1 m, where the initial error was 20 m. After continuous measurements of 4 hours, several hours of non-measurement period comes, because the rover cannot catch the mother spacecraft in sight. In the simulation described in this chapter, the rotational period was 12 hours while the orbit period was 130 hours that it repeats observable time and not-observable time every approximately 6 hours. Simulation results proved that estimation errors in the longitude elements of the position of the rover, which were x and y , decrease in accordance with the rotational motion of the small planetary body, while the estimation error in latitude element, z element, decreases when the mother spacecraft was the pole side. The orbit which pass through the pole region is preferable for accurate localization.

2.5 Analysis on Ambiguities in Motion Parameters

In the previous section, numerical simulations proved that the proposed method of localization can provide sufficiently accurate estimation of the position of the rover under several assumptions. In actual, the ambiguities included in the positions of the mother spacecraft and in the rotational parameters of the small planetary body affects the estimation accuracy. From the reference paper [35], the rotational period of the asteroid Itokawa is estimated with high accuracy as 12.1324 ± 0.0001 hour, where the direction of the rotational motion is estimated with ambiguity of 6.9 deg [36]. This section reports analyses on estimation accuracy under ambiguities in the parameters of rotational motion and positions of the mother spacecraft.
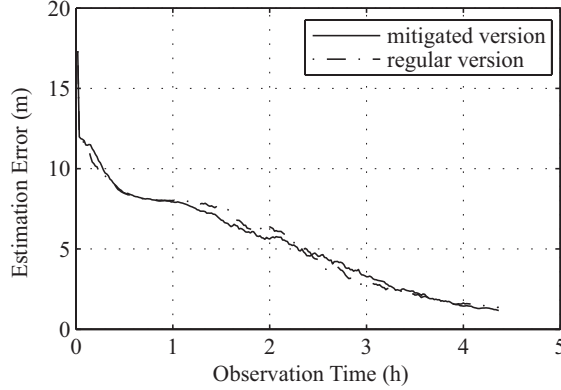
Fig. 2.8: Localization accuracy without estimation of $\boldsymbol{X}_r$: Instead of estimating $\boldsymbol{X}_r$, the mitigated version used the observation data $\boldsymbol{X}_r$ directly.

2.5.1 Sensitivity Analysis of Position Error in Mother Spacecraft

The information about the motion of the mother spacecraft is necessary to predict the position at reception from the position at emission time. If the target planetary body is relatively large, it is feasible to represent the motion of the mother spacecraft by orbit elements. However, for the small planetary bodies of less than 1000 m in diameter, the motion of the mother spacecraft may be difficult to represent by orbit elements because of variations of micro gravity. In actual, the positions of Hayabusa probe were recursively estimated by the images of the terrain of the asteroid surface and the shape model of the asteroid [29]. Numerical simulations were conducted to evaluate the estimation accuracy assuming that the positions of the mother spacecraft instead of motion information were known. The simulation parameters were the same with the Table 2.1. The nominal positions of the spacecraft were given by orbit elements as listed in Table2.1, while the actual positions of the mother spacecraft had bias error from the nominal value. The simulation results are plotted in Fig.2.9. The horizontal axis denotes the bias error included in the positions of the mother spacecraft and the vertical axis denotes the estimation error included in the position of the rover. The estimation error in the direction of line-of-sight direction, parallel to x-axis, caused large error compared with the other elements, where these influence were asymmetry. The sensitive directions were almost parallel to the direction of x-element, which influenced the estimation accuracy the most. The asymmetry of estimation error in y-element reflects the rotational motion of the small planetary body and the asymmetry in z-element was caused because
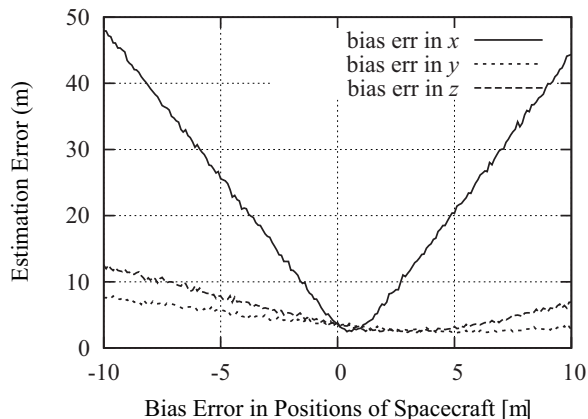
29

Fig. 2.9: Sensitivity analysis with bias errors in spacecraft position

the actual value in z element was -100; the positive error in the position of the mother spacecraft increased sensitivity in z-axis.

Influence of bias error in the position of the mother spacecraft appears in the observation equation, eq. (2.5), which is measurement update step in Kalman filter. In the measurement update step, the estimated state is modified by the innovation between the actual and the estimated measurement. Thus, the ambiguities included in the mother spacecraft can be regarded as ambiguities in measurement. The variance of measurement error, γ, in eq. (2.8), has to include the influence of the ambiguity in the position of the mother spacecraft. In the numerical simulations reported in this chapter, *gamma* was 10^{-16} assuming to represent the processing delay on a transponder. Appropriate variance to represent the influence from the ambiguity in the position of the rover will reduce the influence on localization accuracy of the rover.

2.5.2 Sensitivity Analysis of Direction Error in Rotational Axis

The simulation results assuming ambiguities in the angular velocity, and the direction of the rotational axis of the small planetary body are plotted in Fig. 2.10 and Fig. 2.11, respectively. Ambiguities in the rotational parameters were assumed to have bias error from the nominal values. In both figures, the horizontal axis represents the bias error from the nominal value and the vertical axis denotes the estimation error in the position of the rover. Simulation parameters were the same with Table 2.1, and the results after four hours of observation are plotted.

Fig. 2.10 suggests that the error in angular velocity affects little on the localization accuracy while Fig.2.11 suggests that the bias error in the direction of the rotational axis cause large error in estimation. In the following discussion, the error in the rotational axis
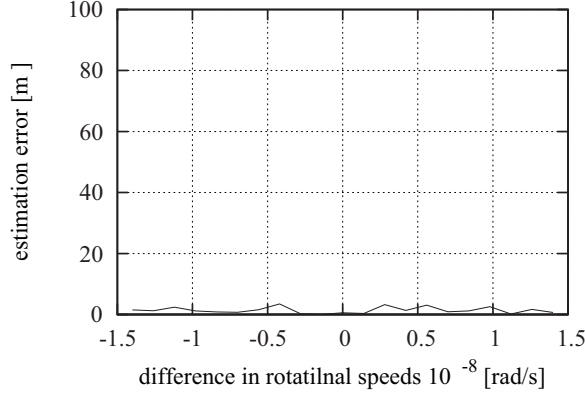
Fig. 2.10: Sensitivity analysis with error in angular velocity

is focused on. For the small planetary body of asteroid Itokawa-size, the bias error of 4 deg of the direction of the rotational axis causes approximately 10 m error in estimation, which is not ignorable. For the recursive method of localization, the direction of the rotational axis of the small planetary body has to be estimated precisely. The simulation results suggests that recursive method of localization with meter-order requires accuracy with less than 1 degree for the direction of the rotational axis of the small planetary body.

Influence from the ambiguities in the rotational period and the direction of the rotational axis appear in the state update of the position of the rover, eq. (2.1). Thus, the ambiguities included in the rotational motion is regarded as prediction error in the position of the rover. The matrix, $\boldsymbol{Q}$, which is the covariance matrix of prediction error, eq. (2.15), need to consider the influence of ambiguities in rotational motion. In the numerical simulations described in this chapter assumed that the motion of the small planetary body to be precisely known, so the covariance matrix, $\boldsymbol{Q}$ was set to $\boldsymbol{0}$. Appropriate covariance matrix, $\boldsymbol{Q}$, will reduce the influence of the ambiguities in the parameters of rotational motion. The problem is how to define $\boldsymbol{Q}$.

2.6 Recursive Method to Reduce Influence of Ambiguities in State Prediction

Let us consider a linear equation of motion,

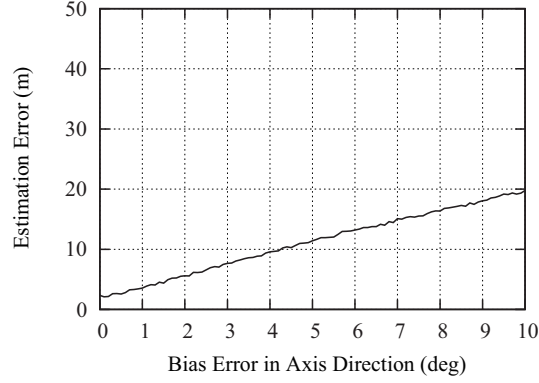$$\boldsymbol{x}(t+1) = \boldsymbol{A}\boldsymbol{x}(t) \tag{2.32}$$

Fig. 2.11: Sensitivity analysis with direction errors in rotational axis

and estimation error $\boldsymbol{e}(t)$ of the parameter $\boldsymbol{x}(t)$, which satisfies

$$E[\boldsymbol{e}(t)] = \boldsymbol{0} \qquad \text{and} \qquad (2.33)$$

$$V[\boldsymbol{e}(t)] = \boldsymbol{P}, \qquad (2.34)$$

where $E[x]$ and $V[x]$ means the average and the variance of x, respectively. Based on eq.(2.32), the prediction error $\boldsymbol{e}(t+1)$ can be described as

$$E[\boldsymbol{e}(t+1)] = \boldsymbol{0} \qquad \text{and} \qquad (2.35)$$

$$V[\boldsymbol{e}(t+1)] = \boldsymbol{A}\boldsymbol{P}\boldsymbol{A}^{T}. \qquad (2.36)$$

If parametric ambiguities are included in the equation of motion as

$$\boldsymbol{x}(t+1) = \boldsymbol{A}^{*}\boldsymbol{x}(t) \qquad (2.37)$$

$$= (\boldsymbol{A} + \Delta\boldsymbol{A})\boldsymbol{x}(t), \qquad (2.38)$$

approximations of the average and the variance of the prediction error $\boldsymbol{e}^{*}(t+1)$ can be expressed as

$$E[\boldsymbol{e}^{*}(t+1)] = \boldsymbol{0} \qquad \text{and} \qquad (2.39)$$

$$V[\boldsymbol{e}^{*}(t+1)] = \boldsymbol{A}\boldsymbol{P}\boldsymbol{A}^{T} + \Delta\boldsymbol{A}\boldsymbol{P}\boldsymbol{A}^{T} + \boldsymbol{A}\boldsymbol{P}\Delta\boldsymbol{A}^{T}. \qquad (2.40)$$

As eq.(2.40) tells, ambiguities in equation of motion, $\Delta\boldsymbol{A}$, increases the variance of the prediction error. We need to take into account this effect of ambiguities.

2.6.1 Estimation Strategy Coping with Uncertainties

Let us define the increased variance of the prediction error in eq.(2.40) as

$$\Delta\boldsymbol{Q} = \Delta\boldsymbol{A}\boldsymbol{P}\boldsymbol{A}^{T} + \boldsymbol{A}\boldsymbol{P}\Delta\boldsymbol{A}^{T}. \qquad (2.41)$$

If we could find upper limit of $|\Delta \boldsymbol{Q}|$ then set a matrix $\boldsymbol{Q}_M$ as

$$|\boldsymbol{Q}_M| \geq \max |\tilde{\boldsymbol{Q}}|, \tag{2.42}$$

which means $\boldsymbol{Q}_M$ is the worst estimation case, we can take into account the ambiguities in equation of motion, $\Delta \boldsymbol{A}$, by adding the matrix $\boldsymbol{Q}_M$ into variance of the prediction error $V[\boldsymbol{e}(t+1)]$,

$$V[\boldsymbol{e}(t+1)] = \boldsymbol{A}\boldsymbol{P}\boldsymbol{A}^T + \boldsymbol{Q}_M. \tag{2.43}$$

Thus, coping with uncertainties in equation of motion results in the maximization problem of $|\Delta \boldsymbol{Q}|$.

Generally, the rotation matrix $\boldsymbol{R}$ can be expressed in terms of the unit matrix $\boldsymbol{I}$, unit vector $\boldsymbol{\sigma}$, which represents rotation axis, and rotational angle β,

$$\boldsymbol{R}(\boldsymbol{\sigma}, \beta) = \cos\beta \boldsymbol{I} + (1 - \cos\beta)\boldsymbol{\sigma}\boldsymbol{\sigma}^T - \sin\beta[\boldsymbol{\sigma}\times] \tag{2.44}$$

where $[\boldsymbol{\sigma}\times]$ is a skew-symmetric matrix describing the cross product of the vector $\boldsymbol{\sigma}$.

Our problem is to cope with ambiguities of the rotational axis that the estimated equation of motion is $\boldsymbol{A} = \boldsymbol{R}(\boldsymbol{\sigma}, \phi_s)$, while the actual equation of motion is $\boldsymbol{A}^* = \boldsymbol{R}(\boldsymbol{\sigma}^*, \phi_s)$, where ϕ_s denotes rotational angle. $\boldsymbol{\sigma}$ and $\boldsymbol{\sigma}^*$ are unit vectors, which are parallel to the estimated and actual axis of a small planetary body, respectively. The difference between the actual and the estimated direction in the rotational axis is denoted as

$$\Delta\boldsymbol{\sigma} = \boldsymbol{\sigma}^* - \boldsymbol{\sigma} = [\Delta\sigma_x \ \Delta\sigma_y \ \Delta\sigma_z]^T . \tag{2.45}$$

As we defined that z axis in the inertial fixed coordination coincides with the nominal rotation axis,

$$\boldsymbol{\sigma} = [0 \ 0 \ 1]^T \qquad \text{and} \tag{2.46}$$

$$\boldsymbol{\sigma}^* = [\Delta\sigma_x \ \Delta\sigma_y \ 1 + \Delta\sigma_z]^T . \tag{2.47}$$

Then the difference of equation of motion can be expressed as

$$\Delta\boldsymbol{A} = \boldsymbol{A}^* - \boldsymbol{A} \tag{2.48}$$

$$= (1 - \cos\phi_s)\Delta\boldsymbol{\sigma}\Delta\boldsymbol{\sigma}^T + \sin\phi_s\,[\boldsymbol{\sigma}\times] . \tag{2.49}$$

By eq.(2.41) and eq.(2.46), the variance of the prediction error, $\Delta\boldsymbol{Q}$, is described as

$$\Delta\boldsymbol{Q} = (1 - \cos\phi_s)\left\{\boldsymbol{\sigma}\boldsymbol{\sigma}^T\boldsymbol{P}\boldsymbol{A}^T + \boldsymbol{A}\boldsymbol{P}\left(\boldsymbol{\sigma}\boldsymbol{\sigma}^T\right)^T\right\}$$
$$+ \sin\phi_s\left\{[\boldsymbol{\sigma}\times]\boldsymbol{P}\boldsymbol{A}^T + \boldsymbol{A}\boldsymbol{P}[\boldsymbol{\sigma}\times]^T\right\} . \tag{2.50}$$

The problem has resulted in maximization $|\Delta \boldsymbol{Q}|$ with constraints,

$$|\boldsymbol{\sigma}^*| = 1 \qquad \text{and} \qquad (2.51)$$

$$\boldsymbol{\sigma} \cdot \boldsymbol{\sigma}^* \leq \cos \theta_a, \qquad (2.52)$$

where θ_a is the maximum ambiguity of the direction of the rotational axis. Since it is difficult to solve eq.(2.50) under constraints eq.(2.51) and eq.(2.52) analytically, it has to be solved by numerically. As the eq. (2.50) includes the variance matrix $\boldsymbol{P}$, the maximization should be solved at each time update step of Kalman filter.

2.6.2 Sensitivity Analysis of Direction Error in Axis

In Fig. 2.12, the simulation results of estimation error with the direction error in the rotational axis processed by various types of covariance $\boldsymbol{Q}$ are plotted. The horizontal axis represents the direction error of the rotational axis of the small planetary body and the vertical axis represents the estimation error of the rover's position. Fig. 2.12 also plots the estimation error processed by original covariance $\boldsymbol{Q} = \boldsymbol{0}$ in solid line, and by constant covariance $\boldsymbol{Q} = 0.1\boldsymbol{I}$ in chain line and $\boldsymbol{Q} = \boldsymbol{I}$ in dashed line. From Fig.2.12, the additional covariance $\boldsymbol{Q}_M$ has the least error in estimation among constant covariance $\boldsymbol{Q} = 0.1\boldsymbol{I}$ and $\boldsymbol{I}$. Moreover, it is more accurate than the original covariance $\boldsymbol{Q} = \boldsymbol{0}$: 75% error of the original one on average. However, it is not sufficient reduction. We can conclude that even the estimation using the covariance $\boldsymbol{Q}_M$ works, but the performance is not sufficient.

2.6.3 Sensitivity Analysis of Precessional Motion

Estimation accuracy in case that the small planetary body contains precessional motion was evaluated by numerical simulations. The estimation errors with precessional motion of the small planetary body are plotted in Fig. 2.13. The horizontal axis represents the precessional period and the vertical axis represents the estimation error of the rover's position. It is assumed that there is 4 degree of difference between the estimated direction and the actual direction of the rotational axis. The estimation accuracy processed by original covariance, $\boldsymbol{Q} = \boldsymbol{0}$, and constant covariance, $\boldsymbol{Q} = 0.1\boldsymbol{I}, \boldsymbol{I}$ and the proposed covariance, $\boldsymbol{Q}_M$, are plotted in Fig. 2.13.

Fig. 2.13 suggests that estimation using the proposed covariance, $\boldsymbol{Q}_M$, had the best accuracy where the precessional period was long enough, while it became worse where the precessional period was less than 1 year. This is because the influence of the second order term in ambiguities are neglected in eq.(2.37). Even though the difference between the actual and nominal direction of axis is small, ambiguities in the equation of motion increase when the precessional period is short. Therefore we need to consider the higher
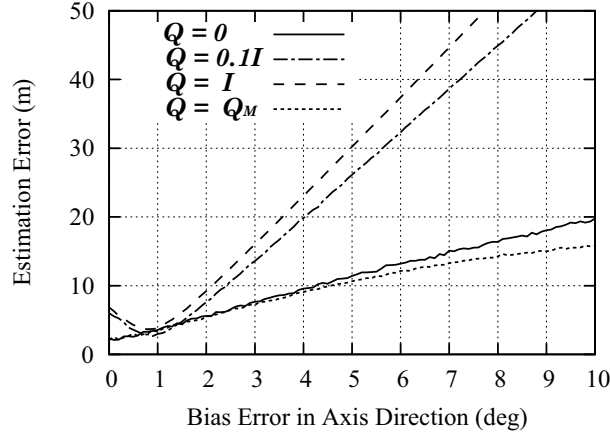
Fig. 2.12: Estimation Error with Covariance $\boldsymbol{Q}_M$ Compared with Conventional Method with Covariance $\boldsymbol{Q} = \boldsymbol{0}$. Although estimation with covariance $\boldsymbol{Q}_M$ has the least error, it is not sufficient reduction.

ordered influence caused by ambiguities in the equation of motion in such case. In actual mission, estimation using $\boldsymbol{Q}_M$ would be enough, because it is difficult to use a rover to investigate such small planetary body with a short period of precessional motion.

2.7 Conclusion

In this chapter, a method of localization for a space rover to guide it to destination points is proposed. Conventional methods of localization cannot be applied to rovers on small planetary bodies of less than 1000 m in diameter. A method of localization has been proposed, which uses measurement of round-trip propagation delay of radio-waves between a rover on a small planetary body and a mother spacecraft orbiting around the small planetary body. In the proposed method, the mother spacecraft is used as a single source of radio waves. The measurement is done repeatedly to make pseudo-multiple reference points of radio sources. Moreover, no synchronization of clocks is needed and no accurate clock is needed on the rover because the proposed method uses the measurements of round-trip propagation delay. The proposed method is able to provide absolute positions of the rover on the small planetary body, and covers the whole surface of the target planetary body, and is applicable to any size of the planetary body.

In this chapter, recursive method to localize a rover has been proposed based on Kalman filter. The estimation accuracy of the proposed method has been evaluated by numerical simulations. The simulation results assuming a rover was located on a
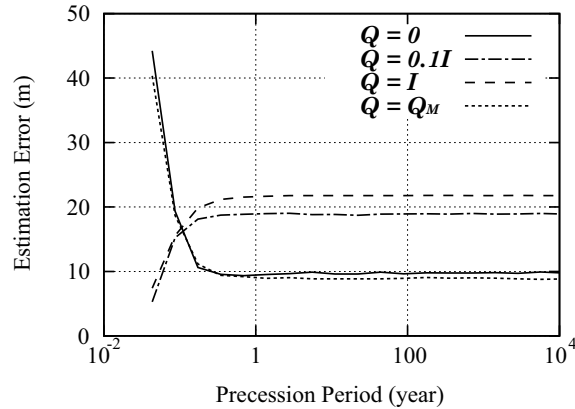
Fig. 2.13: Estimation under Precessional Motion : Where the precessional period is long enough, estimation error becomes constant in each case.

small planetary body proved that the proposed method can provide sufficiently accurate localization of the rover. The influence of ambiguities in rotational motion of the small planetary body and in the positions of the mother spacecraft on estimation accuracy were analyzed. The simulation results proved that the influence from the ambiguity in the angular velocity of the small planetary body is small while the ambiguity in the direction of the rotational axis causes large error in localization. Recursive method to cope with the ambiguities in the rotational motion has been proposed. The proposed method is to increase the covariance matrix of prediction error, Q, appropriately, considering the worst case in prediction under the uncertainties. Simulation results have proved that the proposed method to increase the covariance matrix Q appropriately can reduce the influence of ambiguity, both for the bias error in the rotational direction and for the precessional motion of the small planetary body, however, the performance of influence reduction is not sufficient.

Chapter 3

Estimation Method of Rotation Parameters of a Small Planetary Body and Position of a Rover based on Measurements of Round-trip Propagation Delay

3.1   Introduction

In chapter 2, a method to localize the rover on a small planetary body by a single source of radio-waves has been proposed. This method estimates the position of the rover by using the information about the rotational motion of the small planetary body and the measurements of round-trip propagation delay of radio-waves. The proposed method provides the absolute position of the rover on the small planetary body and covers the whole surface of the target planetary body, and is applicable to any size of the planetary body. In addition, no atmospheric delay, which is one of the largest cause in GPS, will occur on the surfaces of the small planetary bodies so the accuracy of range measurements on a small planetary body would be sufficiently high. Since communication devices on the rover and on the spacecraft can be used for the measurement, only a transponder on the rover is required for the proposed method to work.

This method of localization assumed that the rotational motion of the small planetary body is precisely known. However, the asteroid Itokawa for example, the angular velocity of rotation is estimated as 12.1324±0.0001 h [35] by ground observation, and the rotational direction is estimated with ambiguity of 6.9 deg from the observation by Hayabusa probe [36]. Thus, it is not practical to assume that the rotational motion of the small planetary body to be precisely known. Numerical simulations assuming a rover

is located on the asteroid of 600 m in diameter suggested that an error of 1 deg in the rotational axis direction causes several meters of error in the rover's position.

In this chapter, a method to estimate the rotational parameters of the small planetary body together with the position of the rover is proposed. Estimation method of the rotational parameters is formulated as an optimization problem. Normal method based on gradient is useless to solve this optimization problem because the loss function has different scales of sensitivity to each state variable. In order to avoid this problem, minimum search based on the gradient was divided into three steps. Numerical simulations assumed a rover was located on a small planetary body are shown to evaluate the estimation accuracy of the proposed method. Discussions about the sensitivity direction of the proposed method are also described here. Section 3.2 describes the formulation of the optimization problem and section 3.3 summarizes simulation results, which evaluate the estimation accuracy of the proposed method. In section 3.4, discussions on the sensitivity direction of the proposed method are described, and the section 3.5 concludes this chapter.

3.2 Estimation of Rotational Parameters of Planetary Body and Position of Rover

3.2.1 Overview of Investigations by Rover on Small Planetary Body

Direct investigations into a planetary body using a rover generally follow the four steps below [36].

- Step 1: A mother spacecraft carrying the rover reaches to the target planetary body.

- Step 2: The mother spacecraft investigates into the planetary body in details.

- Step 3: The landing point of the rover is determined using the information collected by the mother spacecraft, then the mother spacecraft releases the rover.

- Step 4: The landing point is localized, and guidance toward destination points starts.

Thus, there is a mother spacecraft near the rover and the spacecraft collects data about the target planetary body in advance of releasing the rover. The mother spacecraft is assumed to be used as a radio source in our method of localization. The method is assumed to estimate the landing point of the rover at Step 4, and the recursive method

of localization described in chapter 2 is assumed to be used after the landing point has been determined. A transponder is assumed to be loaded on the rover on-board to reflect the radio waves transmitted from the mother spacecraft. There are four assumptions for our method of localization.

- Assumption 1: The rover does not move during localization. Thus, the motion of the rover depends only on the rotational motion of the small planetary body.

- Assumption 2: The direction of the rotational axis and the angular velocity is time-invariant.

- Assumption 3: The average and variance of processing delay on the transponder on the rover are are known in advance.

- Assumption 4: The relative positions of the mother spacecraft to the small planetary body are known with sufficient accuracy.

In case that the precession period is sufficiently longer than the operational period of the rover and the direction of the rotational axis can be regarded as constant, Assumption 2 is satisfied. The average and the variance of processing delay on the transponder of Assumption 3 are measurable values in advance of the launch of the rocket carrying the spacecraft and the rover that it is feasible assumption. As the relative positions of Hayabusa probe has been estimated by using the shape model of the asteroid Itokawa, images from optical navigation camera, and LIDAR ranging data [28], it is feasible to assume that the relative position of the mother spacecraft to be known.

3.2.2 Formulation as Optimization Problem

The inertial-fixed coordinate frame used is shown in Fig 3.1. The origin coincides with the planetary body's center of mass. The z-axis is the nominal direction of the rotational axis of the small planetary body, and the x-axis is perpendicular to the z-axis and coincides with the longitude of the ascending node of the spacecraft's orbit. The y-axis is perpendicular to these axes and defined by the right-hand rule. $\boldsymbol{x} = [x, y, z]^T$ and $\boldsymbol{X}$ denote the positions of the rover and mother spacecraft, respectively. $\boldsymbol{\sigma} = [\sigma_x, \sigma_y, \sigma_z]^T$ and ω denote the direction of the rotational axis and the angular velocity of the small planetary body, respectively.

To estimate both the position of the rover and rotational motion of the small planetary body, state vector is defined. Although $\boldsymbol{\sigma}$ is a 3-dimensional vector, it has the constraint $\|\boldsymbol{\sigma}\| = 1$. Therefore, two of the components in $\boldsymbol{\sigma}$ are free. As the nominal direction of the rotational axis is $\bar{\boldsymbol{\sigma}} = [0\ 0\ 1]^T$ from the coordinate definitions, where $^-$ denotes
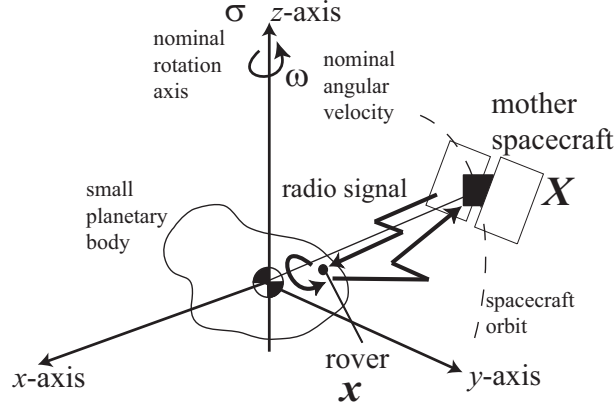
Fig. 3.1: Coordinate Definition

nominal value, σ_z is defined as

$$\sigma_z = \sqrt{1 - \sigma_x^2 - \sigma_y^2} \ . \tag{3.1}$$

Define the state vector $\boldsymbol{s}$ as

$$\boldsymbol{s} = [x, \ y, \ z, \ \sigma_x, \ \sigma_y, \ \omega]^T. \tag{3.2}$$

From Assumptions 1 and 2, the state prediction is derived as

$$\boldsymbol{s}_{i+1} = \begin{bmatrix} \boldsymbol{x}_{i+1} \\ \sigma_{x,i+1} \\ \sigma_{y,i+1} \\ \omega_{i+1} \end{bmatrix} = \begin{bmatrix} \boldsymbol{R}(\boldsymbol{\sigma_i}, \omega_i(t_{i+1} - t_i))\boldsymbol{x}_i \\ \sigma_{x,i} \\ \sigma_{y,i} \\ \omega_i \end{bmatrix} = \boldsymbol{f}(\boldsymbol{s}_i), \tag{3.3}$$

where the suffix i denotes the value at i-th measurement. $\boldsymbol{R}(\boldsymbol{\sigma}, \beta)$ is a rotation matrix and it represents the rotational motion of the planetary body. $\boldsymbol{R}(\boldsymbol{\sigma}, \beta)$ is given as

$$\boldsymbol{R}(\boldsymbol{\sigma}, \beta) = \cos\beta \boldsymbol{I} - \sin\beta \left[\boldsymbol{\sigma} \times\right] + (1 - \cos\beta)\boldsymbol{\sigma}\boldsymbol{\sigma}^T, \tag{3.4}$$

where $\boldsymbol{\sigma}$ and β are the direction of the rotational axis and the angular velocity, respectively [21]. $\boldsymbol{I}$ is a unit matrix and $[\boldsymbol{\sigma} \times]$ is a skew-symmetric matrix representing the cross product of the vector $\boldsymbol{\sigma}$.

The measurement of round-trip propagation delay is expressed as

$$\tau_{ob,i} = g\left(\boldsymbol{s}_i\right) + \zeta_i + \eta_i, \tag{3.5}$$

$$= \frac{1}{c}\left(\|\boldsymbol{X}(t_{e,i}) - \boldsymbol{x}(t_{ref,i})\| + \|\boldsymbol{X}(t_{r,i}) - \boldsymbol{x}(t_{ref,i} + \zeta_i)\|\right) + \zeta_i + \eta_i, \tag{3.6}$$

where c is light speed, ζ_i is the processing delay on the transponder, and η_i is measurement noise of average 0. Using the average of processing delay, $\tilde{\zeta}$, which is a given value from Assumption 4, $(\zeta_i - \tilde{\zeta})$ is a noise component of known variance and of average 0. $\tilde{}$ denotes the average value. The difference in the position of the rover over time $(\zeta_i - \tilde{\zeta})$ is relatively small compared with the distance between the mother spacecraft and the rover, i.e.,

$$\boldsymbol{x}(t_{ref,i} + \zeta_i) \sim \boldsymbol{x}(t_{ref,i} + \tilde{\zeta}), \tag{3.7}$$

where the effect from higher than the second order of $(\zeta_i - \tilde{\zeta})$ is neglected. Thus, the measurement equation (3.6) can be derived as

$$\tau_{ob,i} - \tilde{\zeta} = \frac{1}{c}\left(\|\boldsymbol{X}(t_{e,i}) - \boldsymbol{x}(t_{ref,i})\| + \left\|\boldsymbol{X}(t_{r,i}) - \boldsymbol{x}(t_{ref,i} + \tilde{\zeta})\right\|\right) + (\zeta_i - \tilde{\zeta}) + \eta_i. \tag{3.8}$$

As previously suggested, the average of $(\zeta_i - \tilde{\zeta})$ equals to 0 that this noise component can be regarded to be included in the measurement noise, η_i. In this paper, $\tilde{\zeta} = 0$ for simplicity. $t_{e,i}$, $t_{ref,i}$, and $t_{r,i}$ are the time at emission, at reflection, and the reception of radio waves at the i-th measurement, respectively. These values satisfy

$$t_{ref,i} - t_{e,i} = \frac{1}{c}\|\boldsymbol{X}(t_{e,i}) - \boldsymbol{x}(t_{ref,i})\| \quad \text{and} \tag{3.9}$$

$$t_{r,i} - t_{ref,i} = \frac{1}{c}\|\boldsymbol{X}(t_{r,i}) - \boldsymbol{x}(t_{ref,i})\|. \tag{3.10}$$

The necessary and sufficient condition for locally observability is to satisfy

$$\text{rank}\begin{bmatrix} \dfrac{\partial \boldsymbol{f}}{\partial \boldsymbol{s}_i} - \xi \boldsymbol{I} \\ \dfrac{\partial g}{\partial \boldsymbol{s}_i} \end{bmatrix} = 6 \tag{3.11}$$

for any complex number ξ. In case of $\xi = 1$, the left-hand side of Eq. (3.11) is less than 6, so this system is not locally observable. Recursive approach does not work for estimating the state vector $\boldsymbol{s}_i$.

Let us define the squared error function between the actual measurement, $\tau_{ob,i}$ and the estimation, $\hat{\tau}_i$, as

$$J_{M,i} = \frac{1}{\gamma_i^2}\left(\tau_{ob,i} - \hat{\tau}_i\right)^2, \tag{3.12}$$

where γ_i^2 denotes the variance of the measurement noise, η_i. $\hat{}$ denotes estimation value. From (3.5), $\hat{\tau}_i$ is calculated from the estimated state $\hat{\boldsymbol{s}}_i$ as

$$\hat{\tau}_i = g(\hat{\boldsymbol{s}}_i). \tag{3.13}$$

Thus, $J_{M,i}$ is a function of $\hat{\boldsymbol{s}}_i$. Let us define loss function, J_s, as squared error function of estimation error as

$$J_s(\hat{\boldsymbol{s}}_0) = \sum_{i=0}^{N-1} J_{M,i}(\hat{\boldsymbol{s}}_i). \qquad (3.14)$$

As the state vectors $\hat{\boldsymbol{s}}_i$ $(i = 1, \cdots N - 1)$ are constrained by Eq. (3.3), J_s is expressed as the function of the initial state, $\hat{\boldsymbol{s}}_0$. The maximum likelihood estimation of the initial state $\hat{\boldsymbol{s}}_0^{opt}$ is derived by solving the following optimization problem:

$$\hat{\boldsymbol{s}}_0^{opt} = \arg\min_{\hat{\boldsymbol{s}}_0} J_s(\hat{\boldsymbol{s}}_0) \qquad (3.15)$$

$$\text{subject to} \quad \hat{\boldsymbol{s}}_{i+1} = \boldsymbol{f}(\hat{\boldsymbol{s}}_i). \qquad (3.16)$$

3.2.3 Inequality Conditions from Information about Rotational Parameters

The information about the ambiguities of the rotational parameters of the small planetary body described in the references [35] and [36] is expressed as

$$\bar{\boldsymbol{\sigma}}^T \boldsymbol{\sigma}^* \geq \cos\theta_a \quad \text{and} \qquad (3.17)$$

$$|\omega^* - \bar{\omega}| \leq \omega_a , \qquad (3.18)$$

where * denotes the actual value, θ_a and $\omega_a \geq 0$ denote ambiguities in the direction of the rotational axis and in the angular velocity of the small planetary body, respectively. The actual direction of the rotational axis $\boldsymbol{\sigma}^*$ exists in the cone with axis direction $\bar{\boldsymbol{\sigma}}$ and vertex angle $2\theta_a$, as illustrated in Fig 3.2. The information about ambiguities in rotational parameters is added to the optimization problem, (3.15), as the following inequality conditions:

$$h_\sigma(\hat{\boldsymbol{\sigma}}_i) = \cos(\theta_a) - \bar{\boldsymbol{\sigma}}^T \hat{\boldsymbol{\sigma}}_i \leq 0 \quad \text{and} \qquad (3.19)$$

$$h_\omega(\hat{\omega}_i) = |\hat{\omega}_i - \bar{\omega}| - \omega_a \leq 0. \qquad (3.20)$$

These inequality conditions can be relaxed by applying the augmented Lagrange method [37].

3.2.4 Optimization Based on Gradient

Constraints of motion equation can be relaxed by Lagrange's multipliers as

$$J = J_s + \sum_{i=0}^{N-1} \boldsymbol{\lambda}_{i+1} \{\boldsymbol{f}(\boldsymbol{s}_i) - \boldsymbol{s}_{i+1}\} , \qquad (3.21)$$
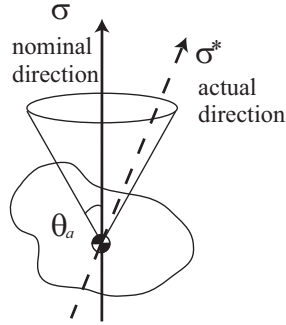
Fig. 3.2: Definition of ambiguity in nominal direction of rotational axis. Actual direction exists within the limited space, expressed as a cone, but the precise direction is not known.

where $\boldsymbol{\lambda}$ denotes co-state. Define Hamiltonian H_i as

$$H_i = J_{M,i} + \boldsymbol{\lambda}_{i+1}^T \boldsymbol{f}(\boldsymbol{s}_i). \tag{3.22}$$

The first derivative of the loss function, dJ, is expressed as

$$dJ = \sum_{i=1}^{N} \left(\frac{\partial H_{i-1}}{\partial \boldsymbol{\lambda}_i} - \hat{\boldsymbol{s}}_i^T \right) d\boldsymbol{\lambda}_i - \boldsymbol{\lambda}_N^T d\hat{\boldsymbol{s}}_N + \sum_{i=0}^{N-1} \left(\frac{\partial H_i}{\partial \hat{\boldsymbol{s}}_i} - \boldsymbol{\lambda}_i^T \right) d\hat{\boldsymbol{s}}_i + \boldsymbol{\lambda}_0^T d\hat{\boldsymbol{s}}_0. \tag{3.23}$$

If the following two equations,

$$\hat{\boldsymbol{s}}_{i+1} = \frac{\partial H_i}{\partial \boldsymbol{\lambda}_{i+1}} = \boldsymbol{f}(\hat{\boldsymbol{s}}_i) \qquad (i = 0, 1, \cdots, N-1) \tag{3.24}$$

$$\boldsymbol{\lambda}_i^T = \frac{\partial J_{M,i}}{\partial \hat{\boldsymbol{s}}_i} + \frac{\partial J_{\sigma,i}}{\partial \hat{\boldsymbol{s}}_i} + \frac{\partial J_{\omega,i}}{\partial \hat{\boldsymbol{s}}_i} + \boldsymbol{\lambda}_{i+1}^T \frac{\partial \boldsymbol{f}}{\partial \hat{\boldsymbol{s}}_i}$$
$$(i = 0, 1, \cdots N-1) \tag{3.25}$$

are satisfied, and the boundary condition,

$$\boldsymbol{\lambda}_N = \boldsymbol{0} \tag{3.26}$$

is satisfied, the first derivative of loss function, J, becomes

$$dJ = \boldsymbol{\lambda}_0^T d\hat{\boldsymbol{s}}_0. \tag{3.27}$$

$\boldsymbol{\lambda}_0$ is the steepest descent direction at $\hat{\boldsymbol{s}}_0$ of the loss function, J. Define the update of state, Δs, as $\Delta s = -\alpha \boldsymbol{\lambda}_0$, then the difference in loss function by updating state, ΔJ becomes $\Delta J = -\alpha \boldsymbol{\lambda}_0^T \boldsymbol{\lambda}_0 < 0$, which provides decrease in loss function. In the simulations represented in this chapter, α was defined by line-search algorithm [38].

3.2.5   Sensitivity Analysis of Performance Index

Before applying the solution based on the gradient, difference in the sensitivities of each variable of state vector has to be considered. Fig. 3.3 plots the values of the loss function according with the difference in individual variables of the state vector, s. The parameters of numerical simulations are the same with chapter 2, as listed in Table 2.1, where the actual state, s_0^*, was set to the nominal state. Change in the value of the loss function according with x, y, z was small while it was large in variables σ_x, σ_y and huge change was occurred in the variable ω. Since the loss function has different scales of sensitivity to six variables of the state vector, minimum-search according with the gradient vector will be trapped in the limited space, which has the highest sensitivity. Then the minimum search following the gradient direction requires many times of iteration to reach the optimal state. The inequality conditions, eq. (3.19) and eq. (3.20) also contribute to reduce the search speed.

In order to avoid to search in the limited space, minimum-search has been divided into three steps. Search algorithm starts in order of sensitivity as follows.

1. Set $s_{\omega,\sigma,x}^1$ as the best known variables and set $l = 1$ and set $ds_\omega = [0\ 0\ 0\ 0\ 0\ 1]^T$.

2. s_ω^{l+1} is determined so that $s_\omega^{l+1} = J(s_{\omega,\sigma,x}^l + \alpha ds_\omega)$ is a minimum.

3. Calculate the gradient and set $ds_\sigma = [0\ 0\ 0\ d\sigma_x\ d\sigma_y\ 0]^T$, which is projected to σ space.

4. $s_{\omega,\sigma}^{l+1}$ is determined so that $s_{\omega,\sigma}^{l+1} = J(s_\omega^{l+1} + \alpha ds_\sigma)$ is a minimum.

5. Calculate the gradient and set $ds_x = [dx\ dy\ dz\ 0\ 0\ 0]^T$, which is projected to x space.

6. $s_{\omega,\sigma,x}^{l+1}$ is determined so that $s_{\omega,\sigma,x}^{l+1} = J(s_{\omega,\sigma}^l + \alpha ds_x)$ is a minimum.

7. Repeat from 2.

3.3   Simulation Results to Evaluate Estimation Accuracy

3.3.1   Brief Overview of Numerical Simulations

Numerical simulations assuming a rover was located on a small planetary body were conducted to evaluate the estimation accuracy of the solution based on Powell's conjugate direction method. The simulation parameters were the same with the simulation reported
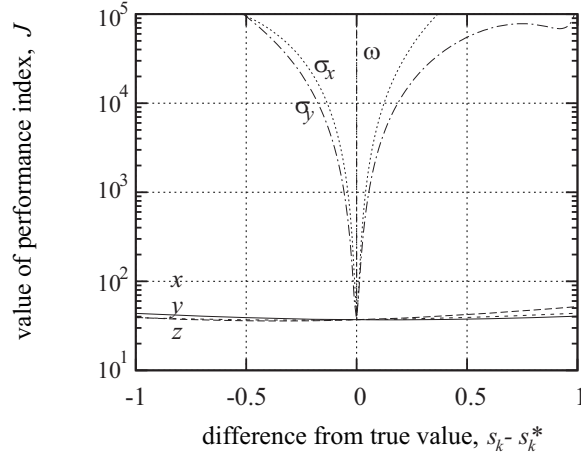
Fig. 3.3: Sensitivity of loss function to each state variable

in chapter 2, as listed in Table 2.1. The prior estimation of the initial state, $\hat{\boldsymbol{s}}_0$, was set to coincide with the nominal state, $\bar{\boldsymbol{s}}_0$. Measurement noise was assumed to be Gaussian with the average of 0 s and the variance of 10^{-16} s^2, which reflected the performance of a recent transponder for space use. Measurement data was collected when the rover could catch the mother spacecraft in sight. The range of view of the rover was assumed to be 1.4 rad from zenith. Ambiguity in the position of the rover was assumed to be 30 m in each direction, x, y and z, which reflected the supposed distance between the target and the actual landing point. The ambiguity in the direction of the rotational axis, θ_a, was 0.17 rad, and the ambiguity in the angular velocity, ω_a, was 4.2×10^{-6} rad/s. These values reflect the information about the ambiguity in the rotational parameters of the asteroid Itokawa [35], [36]. The iteration was set to stop when the decrease in the value of the loss function was less than a threshold, $\Delta J < 10^{-2}$. The following results were provided by the computer with Intel Core i7, 2.93GHz, and Matlab 2009a software.

3.3.2 Evaluation of the Convergence

The convergence of the proposed method has been verified. Measurement interval, ΔT, was 600 s and the observation period, T_N, was 2.16×10^5 s. The actual state, $\boldsymbol{s}_0^*$, was set assuming the maximum uncertainty as

$$\boldsymbol{x}_0^* = (10, 310, -90)^T \tag{3.28}$$

$$\sigma_{x,0}^* = \sigma_{y,0}^* = 0.12 \tag{3.29}$$

$$\omega_0^* = 1.442 \times 10^{-4}. \tag{3.30}$$

The values of the loss function together with the iteration are plotted in Fig. 3.4. The
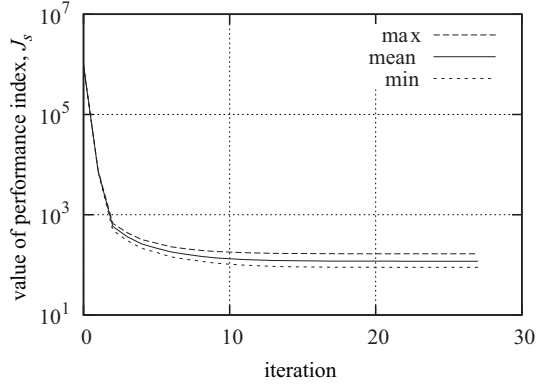
45

Fig. 3.4: Value of performance with iteration : The initial error was fixed

horizontal axis denotes the iteration and the vertical axis denotes the value of the loss function, J_s in (3.14). Fig. 3.4 shows that the value of the loss function, J_s, decreased in accordance with iteration. It tells that the three-step gradient search, described in the subsection 3.2.5, worked appropriately. In Fig. 3.5, the estimation error together with the iteration is plotted. The estimation error is $\|\hat{s}_0 - s_0^*\|$, where $\|\cdot\|$ denotes Euclidean norm. At the end of the iteration, the maximum error in the individual variable of the state vector was

$$[|\hat{x}_0 - x_0^*|, |\hat{y}_0 - y_0^*|, |\hat{z}_0 - z_0^*|] = [1.4, 1.3, 1.3] \tag{3.31}$$

$$|\hat{\sigma}_{x,0} - \sigma_{x,0}^*| = 2.2 \times 10^{-3} \tag{3.32}$$

$$|\hat{\sigma}_{y,0} - \sigma_{y,0}^*| = 3.6 \times 10^{-3} \tag{3.33}$$

$$\cos^{-1}(\hat{\boldsymbol{\sigma}}^T \boldsymbol{\sigma}^*) = 3.9 \times 10^{-3} \tag{3.34}$$

$$|\hat{\omega}_0 - \omega_0^*| = 2.7 \times 10^{-8}. \tag{3.35}$$

Fig. 3.5 shows that the estimation error decreased in accordance with the iteration. We can conclude that the calculation of the proposed method converges to the true state independent from measurement noise.

3.3.3 Validation of Convergence for Various Initial Errors

The convergence for various cases of initial error was verified. Measurement interval, ΔT, and the observation period, T_N, were the same with the subsection 3.3.2, 600 s and 2.16×10^5 s, respectively. 128 cases of initial error were assumed and the values of the loss function and the estimation error in the iteration of optimization were analyzed. Each case of initial error assumed the maximum difference from the nominal state; difference
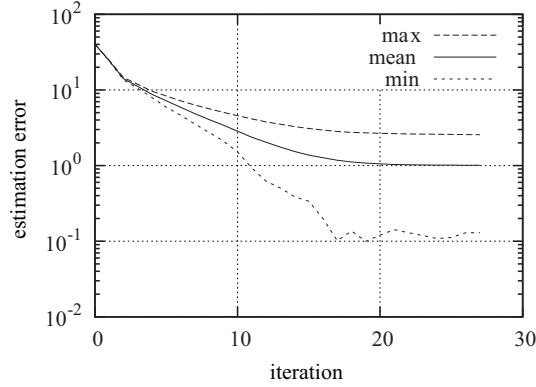
Fig. 3.5: Estimation error with iteration : The initial error was fixed

of $+30$ or -30 in each component of the position of the rover from the nominal value and difference of $+\omega_a$ or $-\omega_a$ in the angular velocity were assumed. For the rotational axis direction, it was assumed to be inclined θ_a from the nominal direction of the rotational axis, and eight directions were considered here for simplicity;

$$\boldsymbol{\sigma}_k^* = \begin{bmatrix} \sin \delta_k \sin \theta_a \\ \cos \delta_k \sin \theta_a \\ \cos \theta_a \end{bmatrix}, \tag{3.36}$$

where $\delta_k = \pi k/4$, $(k = 0, 1, \cdots 7)$. Duration of the measurement, T_N was 2.16×10^5 s. Measurement noise was fixed.

The values of the loss function, J_s, are plotted in Fig. 3.6. The horizontal axis represents the iteration of minimum search and the vertical axis represents the value of the loss function, J_s, (3.14). In the figure, the average, the maximum, and the minimum value of 128 cases of initial error are plotted. The value of loss function decrease in accordance with the iteration, which suggests that the minimum search worked well independent of initial errors.

Estimation error, $\|\hat{\boldsymbol{s}}_0 - \boldsymbol{s}_0^*\|$ is plotted in Fig. 3.7, where the horizontal line denotes the iteration. The average, the maximum and the minimum estimation error of 128 cases of initial error are plotted. As the estimation error is plotted in log-scale, the variation in the minimum estimation error looks relatively large. In actual, the estimation error consisted of position error in the variables, x, y and z, were 10^{-2} order, direction error in the variables, σ_x and σ_y, were 10^{-5} order and the error in the angular velocity, ω, was 10^{-10} order. Thus, the variation in the minimum estimation error is caused by the position error in x, y and z. This order of error satisfies the estimation accuracy described in chapter 2, and it is sufficiently accurate estimation. From Fig. 3.7, the estimation
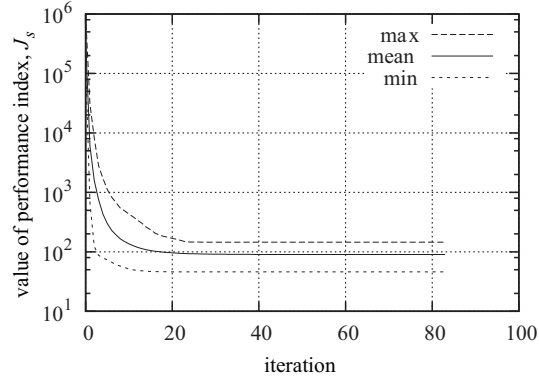
Fig. 3.6: Value of performance index with iteration : Max, mean and min of J_s starting with 128 cases of initial error

error decreased in accordance with iterations. The maximum error in estimation after the iteration was

$$[|\hat{x}_0 - x_0^*|, |\hat{y}_0 - y_0^*|, |\hat{z}_0 - z_0^*|] = [1.7, 3.5, 1.8] \tag{3.37}$$

$$|\hat{\sigma}_{x,0} - \sigma_{x,0}^*| = 2.8 \times 10^{-3} \tag{3.38}$$

$$|\hat{\sigma}_{y,0} - \sigma_{y,0}^*| = 1.3 \times 10^{-2} \tag{3.39}$$

$$\cos^{-1}(\hat{\boldsymbol{\sigma}}^T \boldsymbol{\sigma}^*) = 1.3 \times 10^{-2} \tag{3.40}$$

$$|\hat{\omega}_0 - \omega_0^*| = 7.7 \times 10^{-8}. \tag{3.41}$$

The simulation results proved that the proposed method can provide accurate localization of the rover even if the rotational parameters of the small planetary body contains ambiguities.

3.3.4 Influence of Measurement Interval, ΔT

The influence of measurement interval, ΔT, on estimation accuracy has been evaluated. The observation time, T_N, was set to be the same with the subsection , 2.16×10^5 s. The actual state, $\boldsymbol{s}_0^*$, was fixed to

$$\boldsymbol{x}_0^* = [10, 290, -90]^T \tag{3.42}$$

$$\sigma_{x,0}^* = \sigma_{y,0}^* = 0.12 \tag{3.43}$$

$$\omega_0^* = 1.442 \times 10^{-4}, \tag{3.44}$$

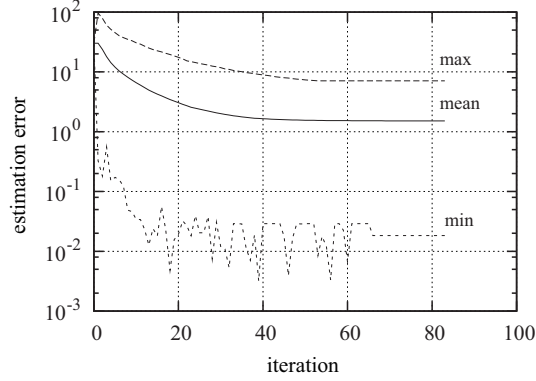which is the worst case in estimation error among 128 cases of actual state.

Fig. 3.7: Estimation error with iteration : Max, mean and min of estimation error starting with 128 cases of initial error

The estimation error together with the measurement interval, ΔT, is plotted in Fig. 3.8. Fig. 3.8 suggests that the estimation error increased in accordance with increase in the measurement interval, ΔT. The values of loss function per number of data, J_s/N, are plotted in Fig. 3.9. The average, the maximum and the minimum values of 100 cases of measurement noise are plotted. The value of J_s/N is useful to judge whether the estimation $\hat{x}$ is close to the actual state or not. If enough measurement data are obtained and the estimation $\hat{x}$ is close enough to the actual state, the estimation error in measurement almost equals to measurement noise and the expected value of J_s/N comes to 1. Fig. 3.9 suggests that in accordance with increase in ΔT, the variance in the value of J_s/N increased, because of the measurement noise. In addition, the average value of J_s/N was less than 1 when ΔT was relatively large, which suggests that the estimated state is trapped to be local minimum. On the other hand, the variance in J_s/N is small and close to 1 when ΔT is relatively small. Thus, the simulation results suggests that the value of loss function per number of measurement data, J_s/N, can be used as an index to judge the estimated state is sufficiently close to the actual state or not.

3.3.5 Influence of Observation Period, T_N

The influence of observation period, T_N, on estimation accuracy was evaluated. The measurement interval was fixed to 600 s. The actual state was the same with section 3.3.4, as represented in equations (3.42), (3.43) and (3.44).

The estimation errors together with the number of measurement, N, are plotted in Fig. 3.10. The horizontal axis denotes the number of measurement, N, and the vertical axis denotes the estimation error, $\|\hat{s}_0 - s_0^*\|$. During the observation period,
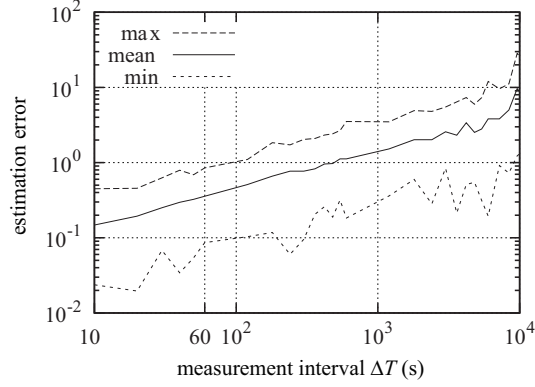
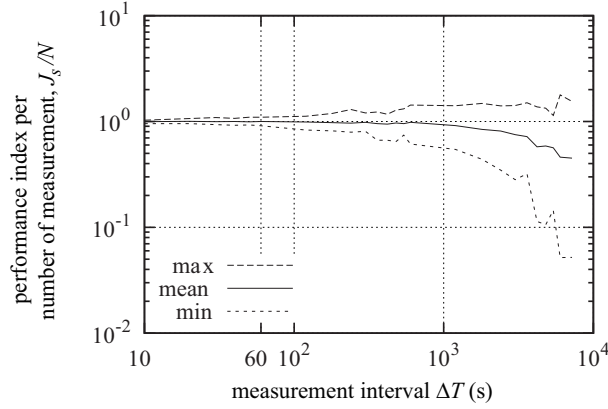Fig. 3.8: Estimation error and measurement interval, ΔT

Fig. 3.9: Value of loss function per number of measurement, J_s/N, with measurement interval, ΔT

T_N, there are $T_N/\Delta T$ chances to collect measurement data, however, the measurement data when the rover cannot catch the mother spacecraft in sight cannot be obtained. To skip the time when no measurement data were collected, the vertical axis is represented by the number of measurement, N, instead of the measurement time, T_N. Fig. 3.10 suggests that estimation error, $\|\hat{s}_0 - s_0^*\|$, decreased in accordance with the number of measurement, N. The sharp drops at $N = 27$ and $N = 43$ coincides the time when the rover lost the mother spacecraft from its sight.

The values of index J_s/N are plotted in Fig. 3.11. The average, the maximum and the minimum values of J_s/N came close to 1 in accordance with the number of measurement data, N, increased. Although the estimation error, $\|\hat{s}_0 - s_0^*\|$, was relatively large at around $N \sim 20$, the average value of index J_s/N was almost 1. The simulation results suggests that only a single index, J_s/N, is insufficient to judge whether the estimated
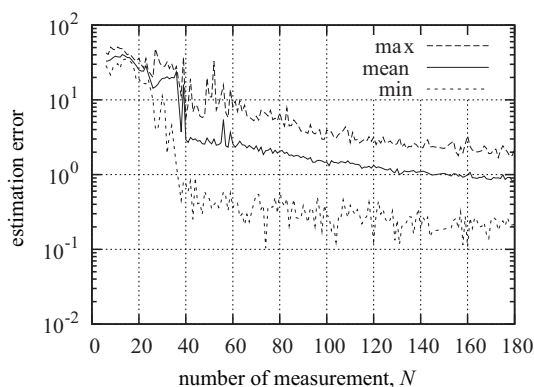
50

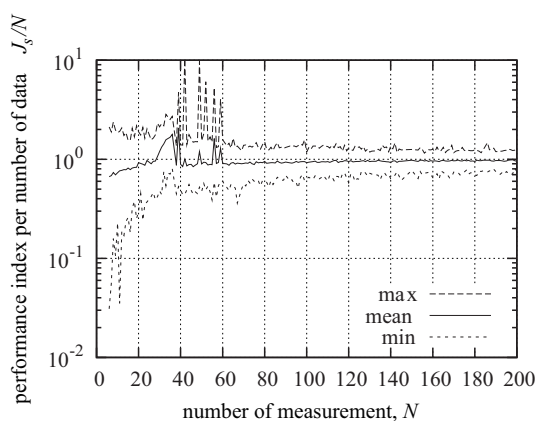Fig. 3.10: Estimation error and number of measurement, N

Fig. 3.11: Value of loss function per number of measurement, J_s/N, and number of measurement, N

state is close to the actual state or not.

3.4 Index of Estimation Accuracy

In section 3.3, applicability of $J_s/N \sim 1$ as an index of accuracy of the estimated state was verified. Simulation results suggested that it was not sufficient index by itself. In this section, the sensitivity direction, $\boldsymbol{b}$, is defined and the performance as an index of estimation accuracy is verified.

3.4.1 Sensitivity Directions of Proposed Method

The localization using measurements based on radio waves has sensitivity in the direction of line-of-sight direction from the source of radio-waves to the receiver. There are two directions of pseudo line-of-sight, which are converted direction of line-of-sight to state space, at i-th measurement of the proposed method; which are

$$\boldsymbol{d}_{e,i}^* = \left(\frac{\partial \boldsymbol{f}_{x,i}}{\partial \boldsymbol{s}_0}\right)^{-1} \frac{\boldsymbol{X}(t_{e,i}) - \boldsymbol{x}^*(t_{ref,i})}{\|\boldsymbol{X}(t_{e,i}) - \boldsymbol{x}^*(t_{ref,i})\|} \quad \text{and} \tag{3.45}$$

$$\boldsymbol{d}_{r,i}^* = \left(\frac{\partial \boldsymbol{f}_{x,i}}{\partial \boldsymbol{s}_0}\right)^{-1} \frac{\boldsymbol{X}(t_{r,i}) - \boldsymbol{x}^*(t_{ref,i})}{\|\boldsymbol{X}(t_{r,i}) - \boldsymbol{x}^*(t_{ref,i})\|}, \tag{3.46}$$

where $\boldsymbol{f}_{x,i}$ represents the function to convert the initial state, $\boldsymbol{s}_0$ to the position of the rover at t_i. $\boldsymbol{f}_{x,i}$ coincides with the prediction of the rover from t_0 to t_i in eq. (3.3), and

$$\boldsymbol{x}_i = \boldsymbol{f}_{x,i}(\boldsymbol{s}_0) = \boldsymbol{R}(\boldsymbol{\sigma}_0, \omega_0(t_i - t_0))\boldsymbol{x}_0. \tag{3.47}$$

Since $\partial \boldsymbol{f}_{x,i}/\partial \boldsymbol{s}_0$ is a 3×6 matrix, eq. (3.45), (3.46) require calculations of pseudo inverse matrix. It is necessary to define the index for estimation accuracy by the values available in estimation calculations. Instead of using the actual position of the rover, $\boldsymbol{x}^*$, the estimated state, $\hat{\boldsymbol{x}}$, was used to calculate the pseudo line-of-sight directions. Moreover, the position difference of the rover and the mother spacecraft during the propagation delay, $\tau_i = t_{r,i} - t_{e,i}$, is relatively small compared with the distance between the rover and the mother spacecraft that the approximation of the pseudo line-of-sight direction at t_i is given as

$$\hat{\boldsymbol{d}}_i = \left(\frac{\partial \boldsymbol{f}_x}{\partial \boldsymbol{s}_0}\right)^{-1} \frac{\boldsymbol{X}(t_{e,i}) - \hat{\boldsymbol{x}}(t_{e,i})}{\|\boldsymbol{X}(t_{e,i}) - \hat{\boldsymbol{x}}(t_{e,i})\|}. \tag{3.48}$$

If a set of N directions of pseudo line-of-sight directions, $\{\hat{\boldsymbol{d}}_i\}$ ($i = 0, 1, \cdots N - 1$), of N measurements are not biased, it will provide accurate estimation. Define a matrix $\boldsymbol{D}$, as a set of pseudo line-of-sight directions as $\boldsymbol{D} = \{\hat{\boldsymbol{d}}_i\}$, where the matrix $\boldsymbol{D}$ is $6 \times N$. Calculate the basis vectors of matrix $\boldsymbol{D}$ by singular value decomposition. Define the left singular vector of matrix, $\boldsymbol{D}$, as $\boldsymbol{u}_k (k = 1, 2, \cdots 6)$ and define the singular value corresponding with the vector $\boldsymbol{u}_k$ as ν_k. The vector $\boldsymbol{u}_k$ is orthonormal basis of a set of line-of-sight directions, and the singular value, ν_k, represents the weight in the direction of $\boldsymbol{u}_k$. The sensitivity direction of the proposed method is defined as

$$\boldsymbol{b} = \sum_{k=1}^{6} \nu_k \boldsymbol{u}_k', \tag{3.49}$$

where $\boldsymbol{u}_k'$ is a vector in which each component is converted to be positive.

Since the value of sensitivity vector $\boldsymbol{b}$ is too large in the direction of the angular velocity, it is difficult to use $\boldsymbol{b}$ directly. We divided the sensitivity vector $\boldsymbol{b}$ into three components, $\boldsymbol{b} = [\boldsymbol{b}_x^T, \boldsymbol{b}_\sigma^T, b_\omega]^T$, in which the components reflect the position of the rover, the direction of the rotational axis, and the angular velocity, respectively. Component b_ω is a scalar value and thus needs no further consideration. If the sensitivity directions $\boldsymbol{b}_x$ and $\boldsymbol{b}_\sigma$ are biased, the estimation results will converge to a local minimum. We define index U to explain the distribution of the sensitivity direction as

$$U = \left\| \frac{\boldsymbol{b}_x}{\|\boldsymbol{b}_x\|} - \frac{1}{\sqrt{3}} \begin{bmatrix} 1 \\ 1 \\ 1 \end{bmatrix} \right\|^2 + \left\| \frac{\boldsymbol{b}_\sigma}{\|\boldsymbol{b}_\sigma\|} - \frac{1}{\sqrt{2}} \begin{bmatrix} 1 \\ 1 \end{bmatrix} \right\|^2 . \tag{3.50}$$

Assuming that the components of the sensitivity direction, $\boldsymbol{b}_x$ and $\boldsymbol{b}_\sigma$, are independent and the averages are equal to $1/\sqrt{3}[1,\ 1,\ 1]^T$ and $1/\sqrt{2}[1,\ 1]^T$, respectively, index U corresponds to the sum of the variance of the distribution of the components $\hat{\boldsymbol{b}}_x$ and $\hat{\boldsymbol{b}}_\sigma$. The averages $1/\sqrt{3}$ and $1/\sqrt{2}$ show that each component in the sensitivity vector, $\boldsymbol{b}_x$ and $\boldsymbol{b}_\sigma$, is distributed uniformly. When index U is close to 0, the components of the sensitivity vector, $\boldsymbol{b}_x$ and $\boldsymbol{b}_\sigma$, are distributed uniformly, which suggests that the estimation result is close to the actual state. In this paper, U is referred to as a uniformity index.

3.4.2 Evaluation of Sensitivity Direction

Numerical simulations were conducted to evaluate the performance of the sensitivity direction, $\boldsymbol{b}$, and the uniformity index, U. The parameters of the numerical simulations were the same with subsection 3.3.5, where the simulation results suggested that the value of index $J_s/N \sim 1$ is not sufficient to judge the accuracy of the estimated state.

The normalized sensitive vector $\boldsymbol{b}_x$ and $\boldsymbol{b}_\sigma$ are plotted in the above figure and the below figure in Fig. 3.12, respectively. The normalization was done at each N. One and the same noise pattern was used. The above figure in Fig. 3.12 suggests that when the number of measurement data was less than 40, z component had less sensitivity. It also suggests that when the number of measurement data was less than 10, σ_y component had less sensitivity. These trends of low sensitivity imply that the estimation may converge to a local minimum. In actual, the estimation error of this simulation results were relatively high in z component and σ_y when the number of the measurement data was less than 40 and less than 10, respectively, which corresponds with the suggestion of the sensitivity vector.

The values of uniformity index, U (3.50) are plotted in Fig. 3.13. The average, the maximum and the minimum value of U of 100 patterns of measurement noise are plotted. Fig. 3.13 shows that U had relatively large value when $N \leq 40$, which indicates that the sensitive vectors were biased. As Fig. 3.10 shows, the estimation error was large when $N \leq 20$. Fig. 3.13 also suggests that once the uniformity index, U, decreased
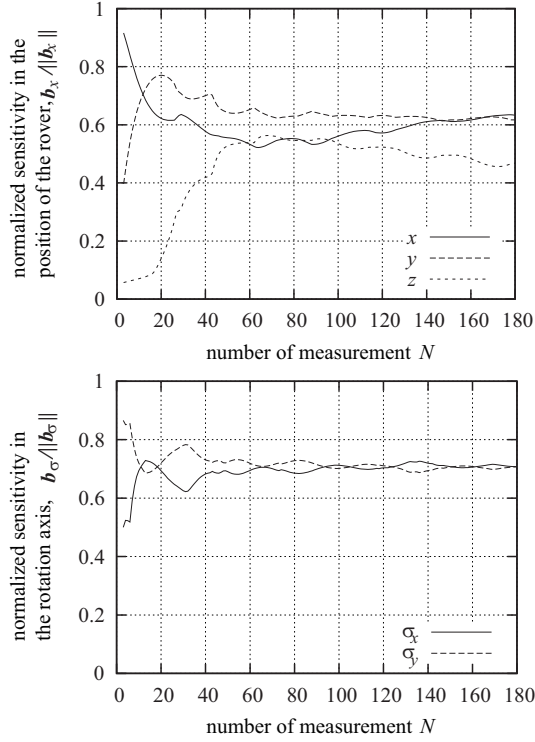
Fig. 3.12: Sensitivity direction with number of measurement, N : (above) normalized sensitivity in the position of the rover (below) normalized sensitivity in the direction of the rotation axis

at $N \sim 4$ then it was relatively large when $N \sim 80$ and $110 < N < 120$. From Fig. 3.10, when the number of measurement data was larger than 40, the estimation error decreases gradually in accordance with the number of measurement data and decrease in estimation error was stationary around $N \sim 80$ and $110 < N < 120$. Thus, we can conclude that the uniformity index, U, can provide information about the convergence of the estimation to the actual state. The rover is ready to move when the uniformity index, U, is sufficiently small.

3.5 Conclusion

In this chapter, a method to estimate the rotational motion of the small planetary body together with the position of the rover has been proposed. The problem includes complex nonlinear and dynamical issues that it cannot be solved analytically. The estimation problem has been formulated as an optimization problem to minimize the loss function defined based on the estimation errors derived in comparison with actual measurement
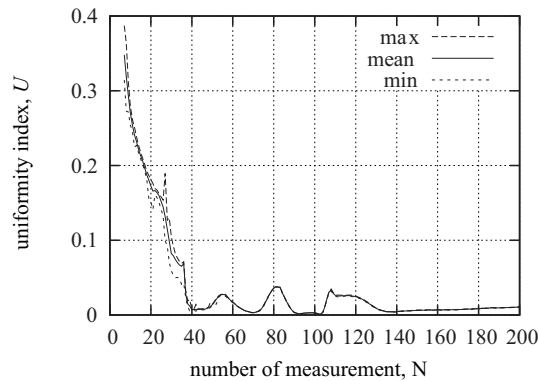
Fig. 3.13: Uniformity index U with number of measurement, N

data. Although this optimization problem can be solved following the gradient vector of the loss function, it takes numerous iteration for optimization because of different scales of sensitivity to each state variable. In this chapter, the optimization following the gradient vector has been divided into three steps. Simulation results proved that the solution of three-step gradient search is able to estimate both the positions of the rover and the rotational parameters with reasonable accuracy. In addition, the influences of measurement interval, ΔT, and of observation period, T_N on estimation accuracy have been evaluated. The sensitivity directions of the proposed method, $\boldsymbol{b}$, has been defined and the uniformity index, U, which represents the distribution of the sensitivity direction has been defined. Numerical simulations proved that the uniformity index represents whether the estimated state is close to the actual state or not.

In this chapter, precessional period was assumed to be much longer than the mission period that influence of precessional motion was neglected. For the problems of this assumption does not work, the index J_s/N won't converge to 1 even sufficient number of measurement data are collected. Thus, the existence of the precessional motion is confirmed. If the influence of precessional motion is included in Eq. (3.4), then estimation considering the precessional motion is achieved.

Chapter 4

Radio-wave Based Accurate Localization of Space Rover without Calculation of Differentials

4.1   Introduction

In chapter 3, a method to estimate both the position of the rover and the rotational motion of the small planetary body using multiple measurements of round-trip propagation delay has been proposed. The method has been formulated as an optimization problem to minimize a loss function defined from the estimation errors derived in comparison with the actual measurement data. This method provides absolute position of the rover in planetary-body-centered frame and covers the whole surface, requiring only a transponder on the rover. Although it can be applied to rovers on any size of planetary bodies, the solution reported in chapter 3 is based on gradient, which requires an accurate and differentiable system model. Therefore, numerical or empirical formula of the motion of the mother spacecraft is not applicable.

In this chapter, a method to solve the estimation problem without calculation of differential is introduced. In spite of calculating differentials, the solution reported here requires a large amount of computation to search the conjugate direction of the loss function. To reduce the amount of computation without loss of estimation accuracy, a methodology to select the measurement data so that the sensitivity directions of the selected data to be conserved is reported in this paper. Numerical simulations assuming a rover is located on a small planetary body and experiments using range measurement tool are shown in this chapter, to evaluate the estimation accuracy and computation time of the proposed method. These results suggest that the proposed solution for localization of a rover on small planetary body using round-trip measurement is effective and generally available.

Mathematical definitions of the optimization problem, sensitivity directions of the proposed method, and the method to select measurement data to conserve sensitivity direction are described in section 4.2. Results from numerical simulations are reported in section 4.3. The experimental results are discussed in section 4.4 and section 4.5 concludes this chapter.

4.2 Accurate Localization of Rovers by Round-Trip Propagation Delay

4.2.1 Solution without Differentials

Powell has proposed a method to find a minimum of a function independent from derivatives [39], which is called Powell's conjugate direction method. The basic algorithm of Powell's conjugate direction method is as following [39], where the function to be minimized is $F(\boldsymbol{p})$, and $\boldsymbol{p}$ is a state vector. $\boldsymbol{\xi}$ has the same dimension with the state vector, $\boldsymbol{s} \in \Re^n$.

1. Determine linearly independent directions $\{\boldsymbol{\xi}_k\}$ ($k = 1, \cdots n$) and set the best known approximation to the minimum, $\boldsymbol{p}_0$ as the starting point.

2. For $k = 1, 2, \cdots n$, calculate λ_k so that $F(\boldsymbol{p}_{k-1} + \lambda_k \boldsymbol{\xi}_k)$ is a minimum, and define $\boldsymbol{p}_k = \boldsymbol{p}_{k-1} + \lambda_k \boldsymbol{\xi}_k$.

3. Find the integer $m(1 \leq m \leq n)$, so that $\{F(\boldsymbol{p}_{m-1}) - F(\boldsymbol{p}_m)\}$ is a maximum, and define $\Delta = \{F(\boldsymbol{p}_{m-1}) - F(\boldsymbol{p}_m)\}$.

4. Calculate $F_3 = F(2\boldsymbol{p}_n - \boldsymbol{p}_0)$, and define $F_1 = F(\boldsymbol{p}_0)$ and $F_2 = F(\boldsymbol{p}_1)$.

5. If either $F_3 \geq F_1$ or $2(F_1 - 2F_2 + F_3) \cdot (F_1 - F_2 - \Delta)^2 \geq \Delta(F_1 - F_2)^2$, use the old directions $\boldsymbol{\xi}_1, \boldsymbol{\xi}_2, \cdots, \boldsymbol{\xi}_n$ for next iteration and use $\boldsymbol{p}_n$ as next $\boldsymbol{p}_0$, otherwise

6. Defining $\boldsymbol{\xi}_{n+1} = \boldsymbol{p}_n - \boldsymbol{p}_0$, calculate λ_{n+1} so that $F(\boldsymbol{p}_n + \lambda_{n+1}\boldsymbol{\xi}_{n+1})$ is a minimum, use $\boldsymbol{\xi}_1, \boldsymbol{\xi}_2, \cdots, \boldsymbol{\xi}_{m-1}, \boldsymbol{\xi}_{m+1}, \cdots, \boldsymbol{\xi}_n, \boldsymbol{\xi}_{n+1}$ as new directions and use $\boldsymbol{p}_n + \lambda_{n+1}\boldsymbol{\xi}_{n+1}$ as the starting point for next iteration.

7. Repeat from 2.

In our problem, the function to be minimized J_s (3.14), and the state vector is $\boldsymbol{s}$ (3.2), which consists of 6 variables, that is $n = 6$. The optimization problem (3.15) is solved by using Powell's conjugate direction method repeatedly as follows:

1. Set the initial state as nominal $\boldsymbol{p}_0 = \bar{\boldsymbol{s}}_0$ and $\boldsymbol{\xi}_k(k = 1, 2 \cdots n)$, to be unit vectors parallel to each axis of state space.

2. Calculate the conjugate direction of the loss function, J_s, following Powell's conjugate direction method. Stop when Δ at the step 3 in Powell's conjugate direction method is less than a threshold, which gives the conjugate direction, $\boldsymbol{\xi}_n$, of the loss function, (3.14) at $\boldsymbol{p}_0$.

3. Update the state $\hat{\boldsymbol{s}}_0^+$ as $\hat{\boldsymbol{s}}_0^+ = \bar{\boldsymbol{p}}_0 + \alpha \boldsymbol{p}_0$ where α is small value so that $J_s(\hat{\boldsymbol{s}}_0^+)$ to be minimum.

4. Set $\hat{\boldsymbol{s}}_0^+$ as $\boldsymbol{p}_0$. Repeat from 2.

It is necessary to set the initial direction to be searched, $\boldsymbol{\xi}$, to be a set of unit vectors because the loss function has different scales of sensitivity to each state variable. Otherwise, the minimum search will require numerous iterations. In the simulation results and the experimental results, α is defined from line-search algorithm in order to guarantee that the loss function decreases monotonically.

4.2.2 Selection of Measurement Data to Reduce Calculation

Although Powell's conjugate direction method can solve the optimization problem (3.15) without calculation of differentials, it requires n different directions of line-search at each iteration to find the conjugate direction of the loss function. Our problem has dynamic condition of the extended state (3.16) that N forward calculations are required for each iteration. Thus, the solution based on Powell's conjugate direction method requires $O(nN)$ amount of computation. The solution described in chapter 3 requires $O(3N)$ amount of computation, since the optimization following the gradient has been divided into three steps. In our problem, $n = 6$ and $n < N$ in general that dominant parameters which increase the amount of computation is the number of measurement data, N. A method to selectively use the measurement data would be effective to reduce the amount of calculation. The problem is which measurement data to use to conserve the estimation accuracy.

In the section 3.4, the uniformity index, U (3.50), has been defined so that the uniformity index represents the distance between the estimated and the actual state. If the measurement data is selected to conserve the value of uniformity index, U, the estimation using the selected measurement data is expected to keep the accuracy. The selection of the measurement data so that the value of uniformity index to be conserved is achieved by following the below steps:

1. Calculate the pseudo line-of-sight directions, $\bar{\boldsymbol{d}}_i$, for each measurement, $i = 0$, 1, $\cdots N - 1$, from the nominal state, $\bar{\boldsymbol{s}}(t_{e,0})$.

2. Define a matrix $\boldsymbol{D}$ as $\boldsymbol{D} = \{\bar{\boldsymbol{d}}_0, \bar{\boldsymbol{d}}_1, \cdots \bar{\boldsymbol{d}}_{N-1}\}$. Derive the base vectors of $\boldsymbol{D}$ by singular value decomposition and define the left singular vectors as $\bar{\boldsymbol{u}}_k (k = 1, 2, \cdots 6)$.

3. Rank the measurement data in order of the distance from each basis, $\|\bar{\boldsymbol{d}}_i - \bar{\boldsymbol{u}}_k\|$. The data which has the smallest distance is ranked in the top.

4. Select the same number of top measurement data from each ranking as representative data.

Although the estimation with less representative data will require less amount of computation for optimization, it is more sensitive to the measurement noise included in the representative data. It is necessary to determine an appropriate number of representative data.

4.3   Numerical Simulations to Evaluate Estimation Accuracy

4.3.1   Parameters for Numerical Simulations

Numerical simulations assuming a rover was located on a small planetary body were conducted to evaluate the proposed solution for the optimization problem. An asteroid was assumed to be spheroid with diameter of $300 \times 300 \times 600$ m, and with uniform density of 2500 kg/m^3. The positions of the mother spacecraft were calculated from orbit elements, which had inclination of 1 rad, semi-major axis of 3×10^3 m and eccentricity of 0.2. The longitude of ascending node, the argument of perigee and the mean anomaly at the beginning of the simulation were all set to 0 rad. The nominal position of the rover at the beginning of the simulation, $\bar{\boldsymbol{x}}_0$, was set $[0, 300, -100]^T$. The nominal direction of the rotational axis and the angular velocity of the small planetary body was $[0, 0, 1]^T$ and 1.4×10^{-4} rad/s, respectively. Ambiguity in the position of the rover was assumed to be 30 m in each direction, x, y and z, which reflected the supposed distance between the target and the actual landing point. The ambiguity in the direction of the rotational axis, θ_a, was 0.17 rad, and the ambiguity in the angular velocity, ω_a, was 4.2×10^{-6} rad/s. These values reflect the information about the ambiguity in the rotational parameters of the asteroid Itokawa [35, 36]. The prior estimation of the initial state, $\hat{\boldsymbol{s}}_0$, was set to coincide with the nominal state. Measurement noise was assumed to be Gaussian with the average of 0 s and the variance of 10^{-16} s^2, which reflected the performance of a recent transponder for space use. The interval of the measurement, ΔT, was 600 s. Measurement data was collected when the rover could catch the mother spacecraft in sight. The range of view of the rover was assumed to be 1.4 rad from zenith. The
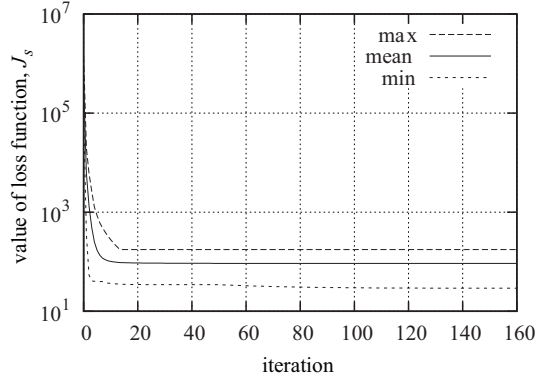
Fig. 4.1: Value of loss function with iteration

iteration was set to stop when the decrease in the value of the loss function was less than a threshold, $\Delta J < 10^{-2}$. The following results were provided by the computer with Intel Core i7, 2.93GHz, and Matlab 2009a software.

4.3.2 Validation of Convergence

To validate the convergence of the optimization by the solution based on Powell's conjugate direction method, 128 cases of initial error were assumed, which were the same cases in subsection 3.3.3, and the values of the loss function and the estimation errors in accordance with the iteration were analyzed. Duration of the measurement, T_N, was 2.16×10^5 s.

   The value of the loss function and the estimation error are plotted in Fig. 4.1 and Fig. 4.2, respectively. In these figures, the average, the maximum and the minimum values of 128 cases of initial error are plotted. Fig. 4.1 shows that the value of loss function decreased in accordance with the iteration, which suggests that the minimum search based on Powell's conjugate direction method worked for any case of initial error. Fig. 4.2 shows that the estimation error decreased in accordance with the iteration. The maximum error in the estimation among 128 cases of initial error was $\|\hat{s}_0 - s_0^*\| = 10.8$, which consists of position error of 10.8 m, direction error of 3.90×10^{-2} rad and error in the angular velocity of 8.34×10^{-8} rad/s. Thus, the rotational parameters of the small planetary body had been estimated with high accuracy. Using the estimated motion of the small planetary body, the method of localization based on Kalman filter can provide the position of the rover with sufficiently high accuracy in real-time. We can conclude that the optimization based on Powell's conjugate direction method provides sufficiently accurate estimation both for the position of the rover and for the rotational parameters of the small planetary body.
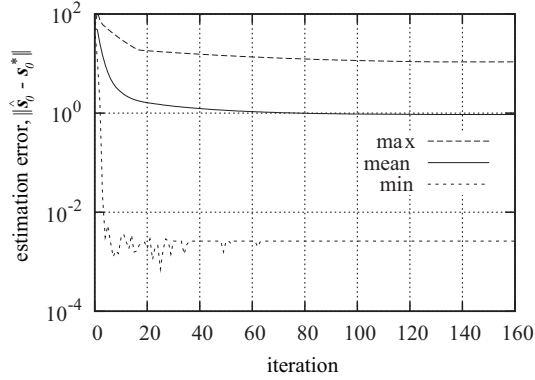
Fig. 4.2: Estimation error with iteration

4.3.3 Validation of Performance of Uniformity Index

In advance of validation of the proposed method to select the measurement data, the performance of the uniformity index calculated from the nominal state, $\bar{U}$, was verified. First, the estimation results of the proposed solution were evaluated in accordance with the number of measurement data, N. The actual state, $\boldsymbol{s}_0^*$, was set as

$$
\hat{\boldsymbol{s}}_0 - \boldsymbol{s}_0^* =
\begin{bmatrix}
\hat{x}_0 - x_0^* \\
\hat{y}_0 - y_0^* \\
\hat{z}_0 - z_0^* \\
\hat{\sigma}_{x,0} - \sigma_{x,0}^* \\
\hat{\sigma}_{y,0} - \sigma_{y,0}^* \\
\hat{\omega}_0 - \omega_0^*
\end{bmatrix}
=
\begin{bmatrix}
-30 \\
-30 \\
-30 \\
-\sin\theta_a \\
0 \\
-\omega_a
\end{bmatrix}
, \tag{4.1}
$$

which was the worst case among the results of 128 cases of initial error. Estimation was simulated on 100 patterns of measurement noise.

The estimation error and the computation time required in the proposed solution are plotted in Fig. 4.3 and Fig. 4.4, respectively, together with the number of measurement data, N. The average, the maximum and the minimum results of 100 patterns of measurement noise are plotted. Fig. 4.3 suggests that estimation error decreased in accordance with the number of measurement data, N. Fig. 4.4 suggests that the required computation time increased largely in accordance with the number of measurement data, N.

The values of uniformity index calculated from the nominal state, $\bar{U}$, are plotted in Fig. 4.5. $\bar{U}$ was relatively large when $N \leq 20$, which coincides with large error shown in Fig. 4.3. $\bar{U}$ decreased in accordance with N, and was almost constant and was approximately 10^{-2} when $N \geq 200$, where the estimation error was relatively small as shown in Fig. 4.3. Thus, the values of uniformity index, $\bar{U}$, reflects the estimation error.
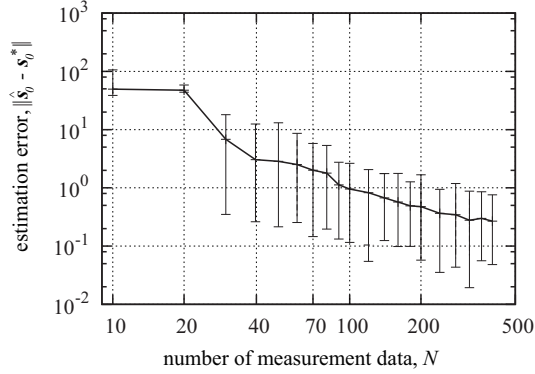
62

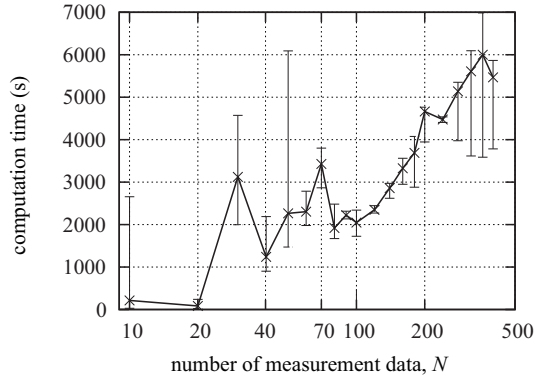Fig. 4.3: Estimation error and number of measurement data

Fig. 4.4: Computation time and number of measurement data

We can conclude that the uniformity index, $\bar{U}$, even if it is calculated from the nominal state, can be used as a reference value to judge the distance between the estimated and the actual state: When $\bar{U}$ is small, the estimated state is expected to be close to the actual state.

4.3.4 Validation of Estimation Accuracy using Selected Data

The performance of the proposed method to select the measurement data was verified in estimation accuracy and computation time by numerical simulations. The actual state was set to be the worst case (4.1), and 100 patterns of measurement noise were simulated. The number of measurement data, N, was set to 200, since the estimation error of the results described in subsection 4.3.3 was sufficiently small and almost constant when $N \geq 200$. The estimation results based on the proposed method of selection were compared with the ones using the data with equal interval of time.
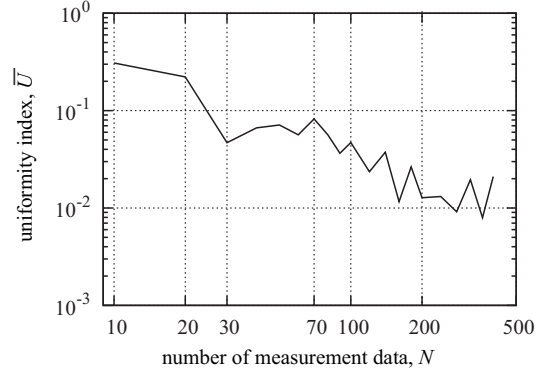
Fig. 4.5: Uniformity index, $\bar{U}$, with the number of measurement, N
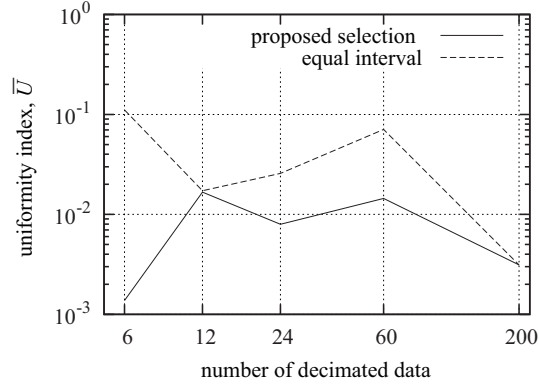

Fig. 4.6: Uniformity index $\bar{U}$ of the proposed method of selection
and of equal interval:

The values of uniformity index calculated from the nominal value, $\bar{U}$, are plotted in
Fig. 4.6. The horizontal axis denotes the number of decimated data. The solid line
denotes the uniformity index $\bar{U}$ calculated by the decimated data using the proposed
method of selection and the dashed line denotes the one calculated by using the data
with equal interval. Fig. 4.6 suggests that the difference of $\bar{U}$ with respect to the number
of decimated data using the proposed method was smaller than the one using the data
with equal interval. It proves that the proposed method to select the measurement data
in order of the norm to the basis of sensitive directions, u_k, conserved $\bar{U}$ as expected.

Estimation error and the computation time using the decimated data are plotted in
Fig. 4.7 and Fig. 4.8, respectively. In theses figures, the solid line and dashed line denote
the estimation results using the decimated data by the proposed method of selection and
ones using the data with equal interval, respectively. From Fig. 4.7, the results using
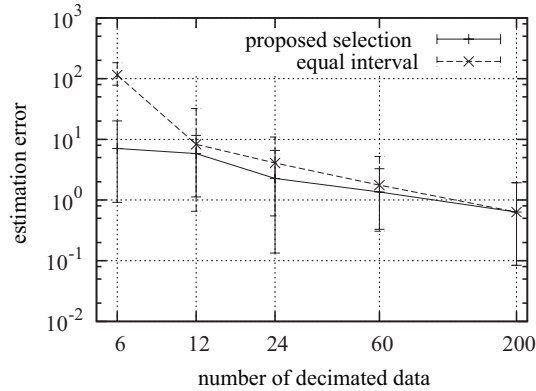the proposed method of selection had smaller error and required less computation time

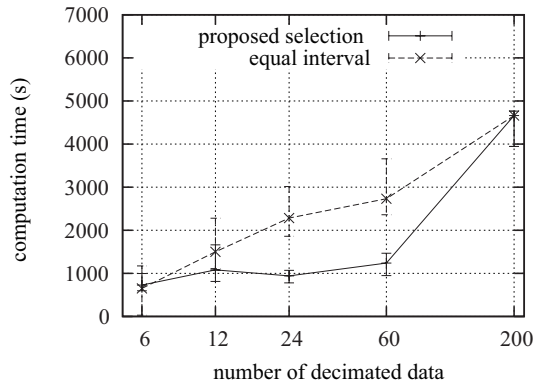Fig. 4.7: Estimation errors of decimated data.

Fig. 4.8: Computation time of decimated data

than the results using the data with equal interval. The estimation error in the results using the proposed method of selection was still 10^0-order while it required less than a quarter amount of computation time of the calculation using the whole data. We can conclude that the proposed method to select data to conserve $\bar{U}$ can effectively reduce the computation time, even though it can provide as accurate estimation as the results using the whole data.
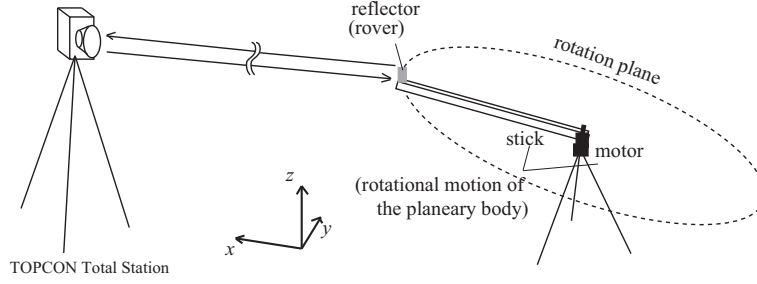
65

Fig. 4.9: Experimental equipments for range measurement : TOPCON Total Station GTS-810A

4.4 Experimental Results using Range Measurement Tool

4.4.1 Overview of Experiments

To show the feasibility of the proposed method, simple experiments using a range measurement tool had been conducted. One end of a straight stick was equipped to a pan-tilt unit (PTU), which simulated the rotational motion of the small planetary body. On the other end of the stick, a reflector of cylindrical shape with 1.1×10^{-2} m in diameter and 1.0×10^{-2} m in height was fixed, which was regarded as a transponder on a rover. Total station (GTS-810A) was used to collect range data. It emits infrared light to the reflector and measures the propagation time of light as well as the direction to the reflector and outputs the distance to the reflector as well as the position of the reflector. The experimental setups are illustrated in Fig. 4.9. In the experiments, output data of measured distance ρ was transformed to round-trip propagation delay τ as

$$\tau = 2\rho/c_a \tag{4.2}$$

where c_a is the light speed in air. The total station was fixed and measured the distance to the reflector at 100 different angles of rotation, which were controlled by PTU. Such data was collected at four different points, each of them approximately 5 m away from PTU, and 400 measurement data was collected in total.

4.4.2 Calibration of Experimental System

Prisms were fixed at three different points, $\boldsymbol{O}_1, \boldsymbol{O}_2, \boldsymbol{O}_3$. $\boldsymbol{O}_1$ was located at the center of the rotational plane made by PTU. $\boldsymbol{O}_2$ and $\boldsymbol{O}_3$ were located so that $\boldsymbol{O}_1, \boldsymbol{O}_2$ and $\boldsymbol{O}_3$ were not in line. The center of the rotational plane is expressed as $\boldsymbol{O}_1 = [0, 0, z]^T$, where z represents latitude element of the position of the rover. The system in this experiment,
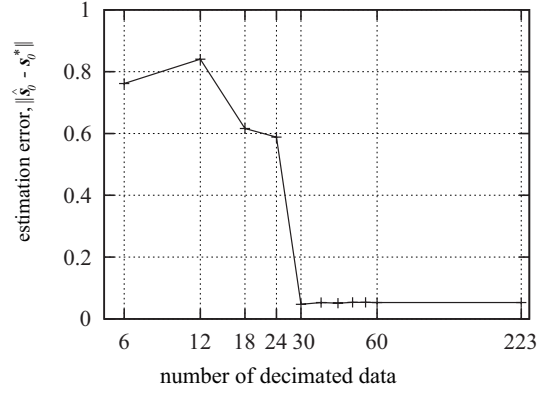
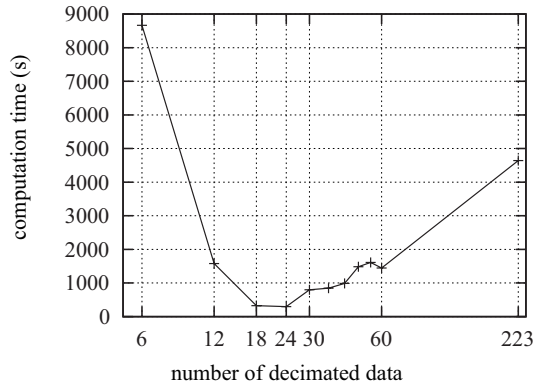Fig. 4.10: Estimation error using experimental data

Fig. 4.11: Computation time using experimental data

z was defined as 0 and the other reference points were $\boldsymbol{O}_2 = [0.7738, -0.6328, -0.0273]^T$ and $\boldsymbol{O}_3 = [0.0959, 0.9394, -0.3293]^T$.

The positions of the total station referred the positions of the prisms. 400 data of the positions of the reflector were used to calibrate the rotational plane. The first and the second component of principal component analysis of the data of the reflector's positions are parallel to the rotational plane, and the third component is parallel to the direction of the rotational axis. The calibrated direction of the rotational axis in the experiment was

$$\boldsymbol{\sigma}_c = [0.3067,\ 0.1490,\ 0.9401]^T, \tag{4.3}$$

which was inclined 0.34 rad from the horizontal plane. The suffix c denotes that the value is calibrated one. The angular velocity, ω_c, was set to be 0.10 rad/s. The position of the reflector at the beginning of the experiment, $\boldsymbol{x}_{c,0}$, was determined to minimize the

67

error between the measured positions and the calculated positions using the calibrated values, $\boldsymbol{\sigma}_c$ and ω_c. Consequently, the initial position of the reflector, $\boldsymbol{x}_{c,0}$, was

$$\boldsymbol{x}_{c,0} = [-0.7837, \ -0.09614, \ 0.2709]^T. \tag{4.4}$$

The difference between the measured and the calculated distance from the calibrated values was 2.383×10^{-4} m in average and the variance was 4.042×10^{-5} m^2. The variance of the difference in distance was used in the estimation as the variance of the measurement noise as $\tilde{\gamma}_i^2 = 4.042 \times 10^{-5}/c_a^2$.

4.4.3   Estimation Results of Proposed Method

The range of the rover's view was assumed to be π rad. Thus, the measurement data τ_i, when the position of the reflector, $\boldsymbol{x}_i$, and the position of total station, $\boldsymbol{X}_i$, satisfy

$$\boldsymbol{x}_i^T \left(\boldsymbol{x}_i - \boldsymbol{X}_i \right) \geq 0 \ , \tag{4.5}$$

was used for estimation. 223 range data out of 400 measurement data were used for estimation. The nominal state at the beginning of experiment was set as

$$\bar{\boldsymbol{x}}_0 = \boldsymbol{x}_0^* + [0.1, \ 0.1, \ 0.1]^T \tag{4.6}$$

$$\bar{\boldsymbol{\sigma}} = [0, \ 0, \ 1]^T \tag{4.7}$$

$$\bar{\omega} = \omega^* - 0.03, \tag{4.8}$$

where the calibrated values, $\boldsymbol{x}_{c,0}$, $\boldsymbol{\sigma}_c$, ω_c, were used as $\boldsymbol{x}_0^*$, $\boldsymbol{\sigma}^*$, ω^*, respectively, and $\bar{\boldsymbol{x}}_0$ and $\bar{\omega}$ were defined so that the error rate $(\hat{\boldsymbol{x}}_0 - \boldsymbol{x}_0^*)/\|\boldsymbol{x}_0^*\|$ and $(\hat{\omega} - \omega^*)/\|\omega^*\|$ to be almost the same with the ones in the numerical simulations.

Estimation error and computation time required in estimation are plotted in Fig. 4.10 and Fig. 4.11, respectively. In these figures, the estimation results using the whole 223 measurement data and the ones using the decimated data by the proposed method of selection are plotted. The iteration was set to stop when the value of the loss function per number of measurement, J/N, is less than a threshold, 10^{-3}. Fig. 4.10 suggests that the estimation results using more than 30 data provided as accurate estimation as the estimation using 223 data. Fig. 4.11 suggests that estimation using 18 $\sim$60 data required only a quarter amount of computation time of the calculation using the whole data, while estimation using 6 or 12 data required much more iterations. The reason is that influence of measurement noise became larger, which made it more difficult to optimize. The experimental results proved that the method to select measurement data based on the uniformity index, $\bar{U}$, can reduce the amount of computation if the decimation is not too much.
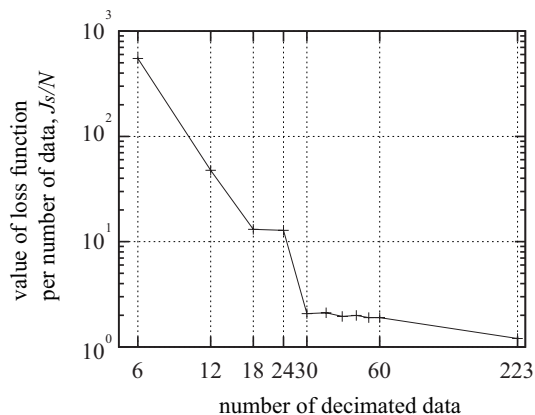
Fig. 4.12: Value of loss function per number of data, J_s/N calculated by using 223 measurement data

In actual, we cannot know the estimation error shown in Fig. 4.10. The index J_s/N, which has been described in subsection 3.3.4, is useful to judge whether the estimation $\hat{s}$ is close to the actual state or not. If the estimation $\hat{s}$ equals to the actual state, then expected value of J_s/N is 1. In case of optimization using the decimated data, the optimal state $\hat{s}^{opt}$ provides the minimum value of index J_s only for these decimated data. If J_s/N using the whole data is close to 1, the optimal state $\hat{s}^{opt}$ of the decimated data would be close to the actual state. This is so called cross-validation. In Fig. 4.12, the values of index J_s/N using the whole 223 data and the estimated state using decimated data are plotted. From Fig. 4.12, the index J_s/N is sufficiently close to 1 when $N \geq 30$, which coincides with the small error in estimation plotted in Fig. 4.10. We can conclude that the index J_s/N using the whole data is effective reference value to check whether the estimated state is close to the actual state.

4.5   Conclusion

In this chapter, a method to estimate the position of the rover together with the rotational motion of the small planetary body has been described. The estimation problem has been formulated as an optimization problem and a solution for the optimization problem has been proposed, which used Powell's conjugate direction method for local search. Although the proposed solution does not require any calculation of differentials, it requires large amount of computation. As the influence of number of the measurement data is significant for the amount of computation, a method to select the measurement data has been proposed in this paper. In order to decimate the measurement data with-

out loss of estimation accuracy, a method to select the measurement data so that the uniformity index, U (3.50) to be conserved is proposed. Numerical simulations assuming a rover was located on a small planetary body and experimental results have proved that the proposed solution can provide sufficiently accurate estimation both for the position of the rover and for the rotational parameters of the small planetary body. The performance of the method to select the measurement data to conserve the uniformity index, U, has been also evaluated. The estimation results using the decimated data by the proposed method of selection have been compared with the results using the decimated data with equal interval. They have proved that estimation using the decimated data by the proposed method can provide more accurate estimation than the estimation using the data with equal interval of time, even it requires less computation time. The experimental results support the feasibility of the proposed method of estimation using round-trip propagation delay of radio waves. The experimental results also proved that the index J_s/N can be used as a reference value to check whether the estimated state is close to the actual state.

Chapter 5

Man-Machine System for Cooperative Control in Uncertain Environment

5.1 Introduction

In the above chapters, a method to estimate the position of the rover on the small planetary body together with the rotational parameters of the small planetary body is described. and estimation accuracy of the proposed method was evaluated by numerical simulations and experimental results. In this chapter, a method to guide a rover on a small planetary body is proposed.

In general, a partly autonomous rover on a small planetary body is guided by an operator on Earth. The operator is able to acquire global information of the small planetary body but the resolution is limited while the rover is able to collect detail information from the on-board sensors but the range of view is limited. Although a method to guide a rover on Mars [40] has been evaluated, it assumes a rover is large and move by wheels. As Yoshimitsu [5] suggested, rovers with wheels are useless on the surface of small planetary body because the gravity is too small to provide enough friction-force to the wheels. Hopping is a promising way to investigate the surface of asteroids, however, the uncertainties in motion prediction is much higher than locomotion by wheels because of ambiguity in the condition of contact and modeling error of the terrain. It is difficult to apply conventional methods to guide a rover such as velocity control and position control. To reach the destination points, the rover and the operator have to merge the information they have and have to cope with the uncertainties of the hopping motion.

In this chapter, a model to guide a hopping rover is proposed. The proposed model is consists of three sub-models, a sub-model of the operator's decision making, a sub-

model of the rover's autonomous control and a sub-model of state prediction. The operator's decision making is modeled as optimization problem of multi-criteria and the operator's preferences of the criteria are shared with the hopping rover. The autonomous control is designed based on multi-criteria problem to select an action which reflects the operator's preference. To cope with the uncertainties in hopping motion, interruptions by an operator is necessary. It is important to present the predicted state of the autonomous robot for the operator so that the operator can understand whether the current strategy in control is appropriate or not. The state prediction of the rover is calculated based on probabilistic approach, which makes easier for the operator to understand the state of the autonomous robot. The section 5.2 describes the proposed model to guide a hopping rover.

The proposed model is applied to a guidance problem of a space rover, and simulation results assuming a hopping rover is located on a small asteroid are reported to show the performance of the proposed system. A hopping rover referred the rover Minerva is assumed and terrain models obtained by the observations of Hayabusa probe are used. These are summarized in section 5.3. The section 5.4 concludes this chapter.

5.2   System Model to Guide Hopping Rover

A mobile robot on remote environment and an operator is assumed and a model to guide the mobile robot under full of uncertainties is proposed. The mobile robot is assumed to be partly autonomous and not to be able to accomplish the task goal without assistance by the operator. The operator is assumed to be able to acquire the information of on-board sensors on the robot, however, limitations on the range of the view of the sensor and on communication capacity makes it difficult for the operator to provide appropriate commands.

Guidance by the operator is regarded as to select a path from numerous paths which link the current state and the goal state of the mobile robot. This type of problems to select a single solution from numerous alternatives is formulated as multi-criteria optimization problems. In multi-criteria optimization problems, a selection of one solution among numerous alternatives depends on a decision maker, which comes from difference in the preferences of each decision maker. By sharing the preferences of the operator with the mobile robot, adaptive action by the autonomous robot will be achieved reflecting the operator's intention. In this chapter, a mobile robot is assumed to be embedded with autonomy to select action which reflect the operator's preferences.

A mobile robot can obtain more detail information than the operator that the action made by the mobile robot may differ from the path-design by the operator. It is important for the operator to interrupt the autonomy when the selected action is not ad-

missible one. So, it is necessary to present the predicted state of the autonomous action of the robot to the operator. The predicted state of the autonomous robot is calculated depending on the selected action and uncertainties in information from on-board sensors. The operator can understand whether the current policy of control is appropriate or not. Especially, it is important to present the uncertainties in prediction to judge whether the influence of uncertainties in environment is admissible or not. So, in addition to the predicted state, the variance in prediction is presented in the proposed system of cooperate control. If the variance in prediction is inadmissible, the operator makes an interruption to change the control policy by changing preferences, and urge the robot to change the action.

The system which includes above ideas is illustrated in Fig. 5.1, which consists of three sub-models. The overview of each sub-system is summarized in below:

Sub-model for Path-Planning by Operator

In general, the control policy of operators does not depend on single criterion but multi-criteria, which in many cases, conflict with each other. Operators have to design priorities in criteria. The decision process of designing priorities is modeled as optimization process of multi-criteria optimization problem. Input of this model is information on environment, which the operator can obtain and outputs are the selected solution and the preferences of the criteria.

Sub-model for Action-Planning by Robot

This model is also based on multi-criteria optimization approach and the optimal solution based on the the operator's preference balance is selected as autonomous action. Inputs are the selected solution by the operator, the preferences and information by on-board sensors. Outputs are action plan of the mobile robot and information obtained by the on-board sensors.

Sub-model for State Prediction

In this model, the state of the mobile robot is calculated using the selected action and the information from on-board sensors, and predicted values of the action for each criterion are also calculated. In many cases, information of environment obtained by on-board sensors contains ambiguities because of performance limitation, it is important to tell the operator the uncertainties included in the estimation explicitly. Inputs are selected action by the mobile robot and the information obtained by the on-board sensors, and outputs are the predicted state of the robot and its variance.
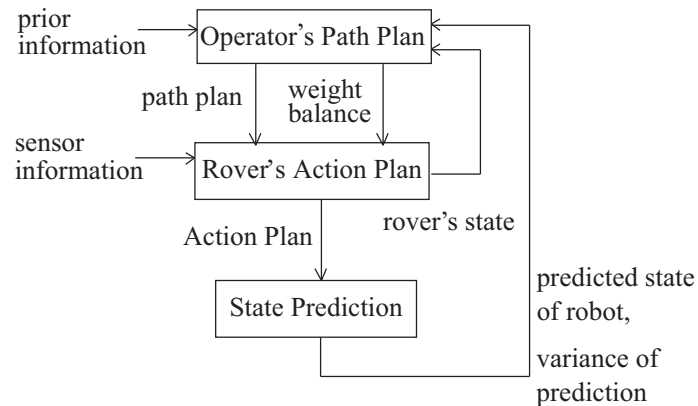
Fig. 5.1: System model to guide a mobile robot with ambiguities in locomotion

5.3 Simulation Results of Guidance Applying Proposed Model

The proposed model to control a mobile robot was applied to a guidance problem of a hopping rover on a small planetary body. The rover Minerva [6] was referred as a hopping rover. In the following, an active jump made by the rover is called a hop, and a passive jump when the rover hit the ground is called a bound.

5.3.1 Preliminaries for Terrain Information

3D shape model of asteroid Itokawa consists of approximately 50,000 data [41] was used for the information for on-board sensors. Taking the average of every 10 data from these data, low resolution of terrain information consists of approximately 5,000 data was used as the information for the operator. The resolution of the information for on-board sensors was 2 m on an average, and the resolution for the operator was almost 20 m. The range of the view of the on-board sensors was set to be 30 m without considering the bump of the surface for simplicity, which was larger than the resolution of the information for the operator. The resolution of the information for the on-board sensors and for the operator are illustrated in Fig. 5.2.

5.3.2 Model of Hopping Motion

By using initial hop-velocity, $\boldsymbol{v}_0$, the facet direction, $h(\boldsymbol{p})$, where $\boldsymbol{p}$ denotes a certain point of terrain, the velocity of the bound of mass point, $\boldsymbol{v}'$, is parallel to the direction
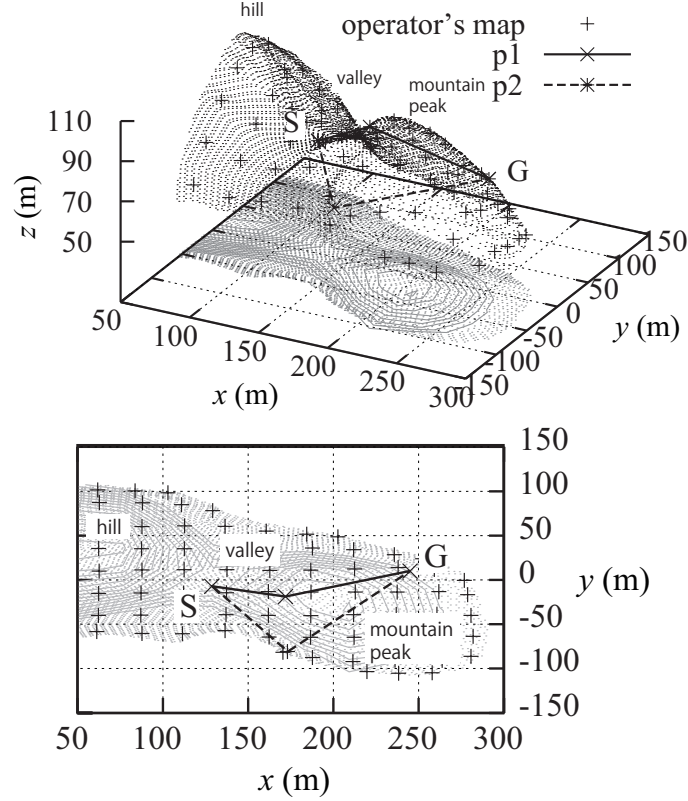
Fig. 5.2: Examples of path-design by operator (above) three-dimensional model (below) top view : Dots in figure above represents actual terrain. + represents operator's low resolution maps. (p1) and (p2) represent path-plan by operator. While (p1) prefers shorter path, (p2) prefers smoother terrain.

of specular reflection. $\boldsymbol{v}'$ is expressed as

$$\left[\begin{array}{c} \boldsymbol{v}'_h \\ \boldsymbol{v}'_v \end{array} \right] = \left[\begin{array}{c} \mu_h(\boldsymbol{p}) \left(\boldsymbol{v}_0 + \boldsymbol{v}_0^T \boldsymbol{n}(\boldsymbol{p}) \right) \\ \mu_v(\boldsymbol{p}) \boldsymbol{v}_0^T \boldsymbol{n}(\boldsymbol{p}) \end{array} \right], \tag{5.1}$$

where suffixes h and v denotes the horizontal and vertical direction to the surface in the plane including $\boldsymbol{v}_0$ and $\boldsymbol{n}(\boldsymbol{p})$, respectively. μ denote the coefficient of restitution of the surface at point $\boldsymbol{p}$.

In a real world problem, predicting a hopping motion, even if the terrain is not uneven, is difficult, because of uncertainties in conditions of contact of the rover and the terrain. A simple model for the bound with uncertainties is given by a diffuse reflection, with average direction $\boldsymbol{v}'$ and a certain variance, ψ_a.

Simulation results of a hopping motion on a flat plane are plotted in Fig. 5.3, assuming diffuse reflection in bound direction. The initial hopping velocity was $\boldsymbol{v}_0 =$
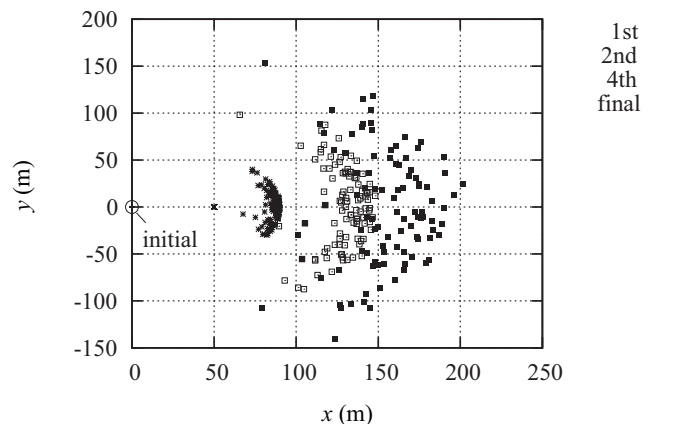
Fig. 5.3: Hopping motion with ambiguity in bound direction: Hopping motion using simple model has been calculated. Initial and final position, and the positions of 1st, 2nd, 4th bound are plotted. The uncertainty in position of the rover increased in accordance with bound, even if plane was assumed to be flat and smooth.

$[0.1, 0, -0.1]^T$ m/s, coefficient of restitution was universe, $\mu_h(\boldsymbol{p}) = \mu_v(\boldsymbol{p}) = 0.8$, and the variance in the bound direction was $\psi_a = 0.35$ rad, where axis z was defined as the gravitational direction. The gravitational force was defined to be 2.6×10^{-5} m/s^2, which reflects the micro-gravity on the surface of asteroid Itokawa at 300 m radius assuming that the mass of the asteroid identically-distributed. The hopping motion was set to stop when the velocity against to the gravitational direction was less than 0.01 m/s. One hundred particles were calculated and the initial and final position, and the positions of 1st, 2nd and 4th bound are plotted in Fig. 5.3. Distribution of the predicted state increased enormously in accordance with the bound even in this simple model, which illustrates the difficulty of precise prediction of the hopping motion.

5.3.3   Feasible Method for State Prediction

As the example described in the subsection, 5.3.2, it is unrealistic to estimate the state of the hopping rover with high accuracy. The paper [42] reported feasible method to calculate non-linear conversion, which is called unscented transformation. It uses representative points called sigma points to deal with the uncertainties included in the state quantitatively. The predicted state of the hopping rover using unscented transformation is plotted in Fig. 5.4, where the same simulation parameters were used with the results illustrated in Fig. 5.3. Four sigma points were used for state calculation considering uncertainties in two axes, x and y. In Fig. 5.4, the average of the state prediction are plotted. Fig. 5.4 shows that the unscented transformation can represent the variance of
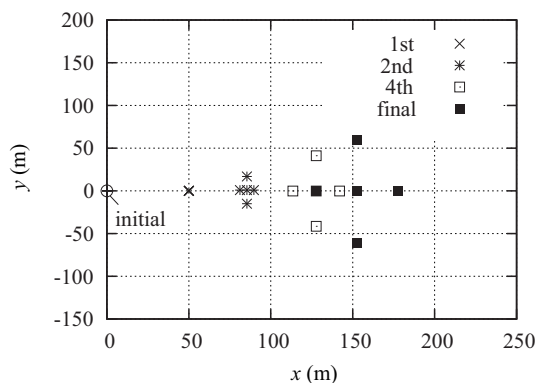
76

Fig. 5.4: State prediction based on unscented transformation: Four sigma points and average state are plotted, where the simulation parameters are the same with Fig. 5.3. Although the Unscented transformation requires small amount of calculation, it illustrates variance in state prediction effectively.

Table 5.1: Comparison of results from unscented transformation and Monte Carlo analysis : the number denotes number of particles used in the analysis.

methodology	average (m)	variance (m)
Monte Carlo:10	(150.8, 5.0)	(59.7, 54.2)
Monte Carlo:100	(160.6, 7.0)	(32.8, 62.9)
Monte Carlo:1000	(161.8, -1.5)	(28.5, 62.7)
Monte Carlo:10000	(161.2, -0.7)	(28.3, 61.5)
Unscented Trans.	(160.7, -0.0)	(28.7, 62.1)

error in the state prediction effectively, which is easier for the operator to understand the ambiguities in prediction than Fig. 5.3. The results using from 10 to 10,000 particles for state prediction and results from unscented transformation are listed in Table 5.1. Although unscented transformation requires a smaller amount of calculation than that of multiple particles, the results were close to the results from 10,000 particles.

5.3.4 Parameters for Multi-Criteria Optimization

The path-plan made by the operator was represented by a set of way points using terrain information of low-resolution. In the simulations, 100 paths were randomly prepared, which had different way points and link the initial and goal state. The number of way points was from 0 to 3.

For the rover's action-plan, 100 alternatives were prepared. Each action-plan specified a hopping velocity, so that the first bounding point made by the hop motion differed with each other. The bounding points were randomly selected by the terrain information of high resolution within the range of view of the on-board sensors.

Three conflicting criteria in guidance were assumed.

1. minimize uncertainties in state

In Fig. 5.5, values at each point on the terrain are plotted, which were defined from the variance of facet directions in local, that is, roughness of terrain. The left figure in Fig. 5.5 shows the distribution of the values calculated from the terrain information of high resolution, while the right figure represents the values calculated from the information of low-resolution. These values at point p are represented as $c_1(p)$ and $\tilde{c}_1(p)$, for the high-resolution and for low-resolution, respectively. The point with thick color represents uneven region and the point with thin color represents smooth region. If the rover bound at the point with thick color, the bounding direction contains large ambiguities that uncertainties in hopping motion will increase, which reduces the accuracy of state prediction.

The value of each alternative for the operator was defined as sum of the parameter values of way points, p_i, that is, $\sum_i \tilde{c}_1(p_i)$. The value of each action-plan of the rover was defined as the value at the first bounding point p, that is, $c_1(p)$.

2. maximize acquirable information values in path

The asteroid Itokawa is spheroidal body and had specific terrains where the curvature was high. SO, another parameter was defined based on the distance from the origin, whose values are plotted in Fig. 5.6. In Fig. 5.6, the left and the right figure represent values calculated from high-resolution and from low-resolution information, respectively, which are denoted as c_2 and $\tilde{c}_2$. The point with thick color represents that it has valuable information to be investigated and the point with thin color represents that it has less value.

The value of each alternative for the operator was defined similar to the criterion 1 as sum of the values of way points, p_i, that is, $\sum_i \tilde{c}_2(p_i)$. The value of each action-plan for the rover was defined as sum of the points p_i, that is, $\sum_i c_2(p_i)$, where p_i is a set of points consists of projection of the hop motion from the current point to the first bounding point.

3. minimize path-length to goal

The last criterion is simple; the shorter is the better. The value of each alternative for the operator was defined as number of way points, since each alternative links
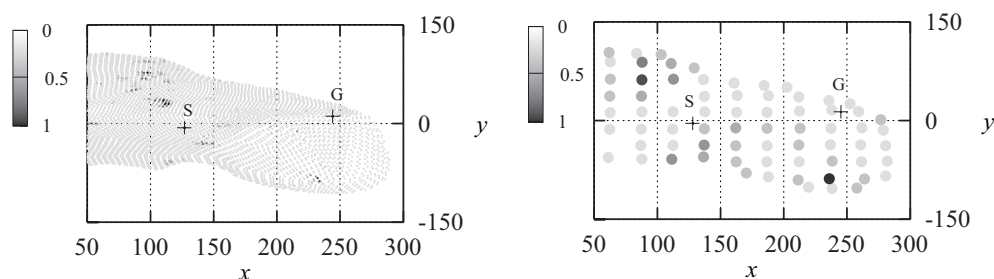
Fig. 5.5: Values Defined from Roughness : (left) detail information for rover, c_1, (right) ambiguous information for operator, $\tilde{c}_1$
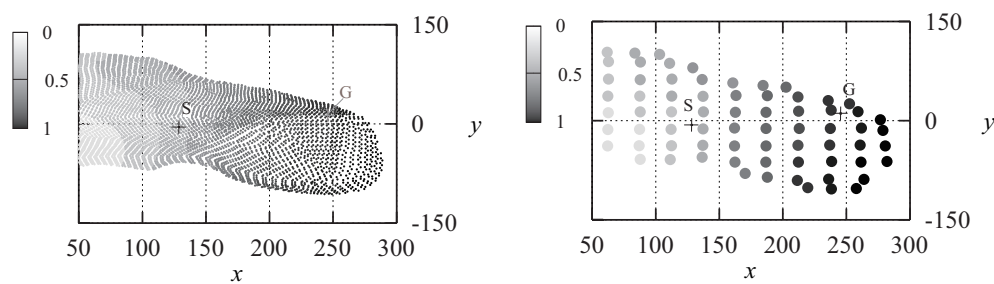

Fig. 5.6: Values Defined from Absolute Position : (left) detail information for rover, c_2 (right) ambiguous information for operator, $\tilde{c}_2$

the initial state and the goal state. The value for the action-plan of the rover was defined from the distance between the first bounding point $\boldsymbol{p}$ to the goal state.

5.3.5 Application Result

Two examples of path-plans made by the operator are plotted in Fig. 5.2, where the initial state and the goal point of the rover are denoted by S and G, respectively. The path p1 reached to the goal state linearly, where the preference balance, w1, had high weight on criterion 3, to minimize the path length. The path p2 was in smooth area and went through the region with high value in $\tilde{c}_2$, where the preference balance, w2, had high weight both on criterion 1, to minimize the uncertainties in prediction, and on criterion 2, to maximize information value.

Two trajectories of autonomous action-plan by the rover without interruption by the operator are plotted in Fig. 5.7. a1 and a2 are the trajectories with the preferences w1 and w2, respectively. The initial velocity, coefficient of restitution and ambiguity
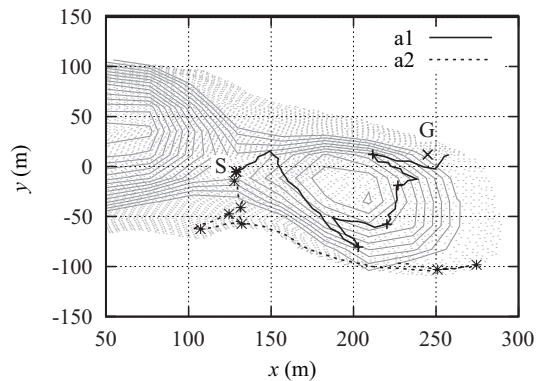
Fig. 5.7: Trajectories of Autonomous Hopping Control by a Rover: (a1) represents a trajectory when path-plan (p1) and preferences (w1) were given and (a2) represents a trajectory when (p2) and (w2) were given. While hop direction of (a1) directly aimed at goal point, G, (a2) selected smoother region, reflecting operator's preferences (w1) and (w2), respectively.

in bound directions were the same with the simulation parameters on smooth plane described in subsection 5.3.2. The gravitational direction was defined to pass through the center of mass. In Fig. 5.7, the locomotion between bounds were projected to xy plane and the projected trajectories are denoted as lines, and the hopping points are denoted by dots. Autonomous action was stopped when the distance to the goal state G was smaller than a threshold, or when the number of hopping was larger than a threshold. The initial hopping motion of the trajectory a1 headed to the goal state, G, reflecting the preference balance, w1, which had high weight on the criterion 3, to minimize the path length. However, the bounding motion made it away from the goal state. The similar motions were found in the subsequent hopping motion, however, the rover was close enough to the goal state, G, in the end. The trajectory a2 reflects the preference balance, w2, where the first hop tried to move smoother regions and the region with higher values to be investigated. It reached to the region with high values in c_2, however, it did not reach the goal state because the number of hop reached to the maximum threshold. This is because the preference on criterion 3, to minimize the distance to the goal point, had low weight that the rover selected the hop velocity which resulted to make the rover to jump toward smooth region and region with high values in information to investigate, instead of heading the goal point. Thus, the action-plans reflected the operator's preferences partially, however, the actual path took a long way or did not reach the goal point, because of the ambiguities in bounding direction.

The state predictions of the rover's actions were calculated by unscented transformation, which are plotted in Fig. 5.8. In the prediction calculations, six sigma points were used assuming that the uncertainty in rover's position distributes in three dimensions. In Fig. 5.8, state predictions of rover's action a1 with the preference w1 are plotted, which suggest that the predicted state covered wide area. Presented these predicted states, the operator made an interruption to the autonomous action: The operator changed the preference balance from w1 to w1', which made change in rover's action from a1 to a1'. The preference balance had lower weight on the criterion 3, to minimize the path length, and had higher weight on criterion 1, to minimize the uncertainty in prediction. State predictions of the rover's action a1' with the preference balance, w1', are plotted in Fig. 5.9. Compared with Fig. 5.8, although the distance to the goal state was longer, the distribution of the predicted state reduced.

Trajectories with interruptions by the operator are plotted in Fig. 5.10 and Fig. 5.11. The trajectory a1' shown in Fig. 5.10 was given starting with the preference balance w1, however, the preference balance was changed to w1', which had higher weight to minimize the uncertainties when the operator obtained the state prediction of Fig. 5.8. Given the preference balance w1', the rover selected the action a1', which was expected to have smaller uncertainties in motion than the action a1. The trajectory a1' was shorter in total compared with the trajectory without interruption, a1. As a result, the trajectory a1 meets the operator's preference. The other example, the trajectory a2' is plotted in Fig. 5.11, where the initial preference balance was w2. At the beginning of the guidance, there was no interruptions and the operator changed the preference balance from w2 to w2' at the middle of the guidance, where the locomotion by the hopping motion was small. The preference balance w2' had lower weight on the criterion 1, to minimize the uncertainties in the motion prediction, and higher weight on the criterion 3, to come to close to the goal state. Another interruption was made at the end of the guidance, after the rover reached to the region with high values in $c2$, the weight on the criterion 3 became higher. In total, the trajectory a2' passed through smoother region, and the region with higher values in $c2$ then reached to the goal state.

Thus, simulation results proved that the proposed model to share the preferences of multi-criteria and to change the preferences dynamically is able to guide a mobile robot with full of uncertainties in locomotion. Unscented transformation was used for complex prediction of the hopping motion, and simulation results suggested that the unscented transformation provides operator-friendly presentation in state prediction and it reduces the amount of computation, which assists the operator to make appropriate interruptions to the autonomous actions.
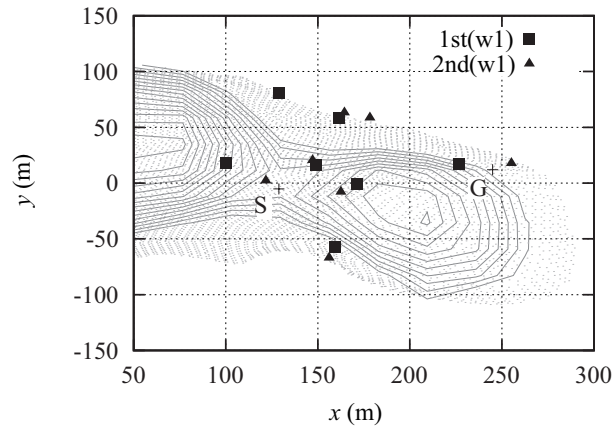
Fig. 5.8: Predicted State from initial action (when preference balance w1 were given) : Hopping direction faces at goal position, G, however, uncertainties in predicted state covers large area.

5.4   Conclusion

In this chapter, a model to guide a mobile robot with full of uncertainties in locomotion has been proposed. The proposed system consists of three sub-models; a sub-model for decision making by an operator, a sub-model for action-plan by an autonomous robot, and a sub-model for state prediction of the robot. The operator's decision making problem has been formulated as an multi-criteria optimization problem and the preferences of criteria were regarded as abstract objective in guidance. In the proposed model, these preferences were shared with the mobile robot so that the autonomous action-plan can reflect the operator's intuition. Even the robot shares the preferences of control criteria, the action made by the robot may differ from the operator's expectation because of uncertainties in locomotion. It is necessary to provide the operator not only the predicted state of the robot by the action-plan but also the variance of the prediction, so that the operator can understand whether the current control policy is appropriate or not. The proposed system was applied to a guidance problem of a hopping rover on a small planetary body. Since the hopping motion is complex because of uncertainties in bounding motion, unscented transformation was used to estimate the predicted state of each action-plan made by the rover together with the variance of estimation, to reduce the amount of computation. The application results have proved that the proposed model effectively realizes a guidance of a hopping rover by realizing appropriate interruptions by an operator.
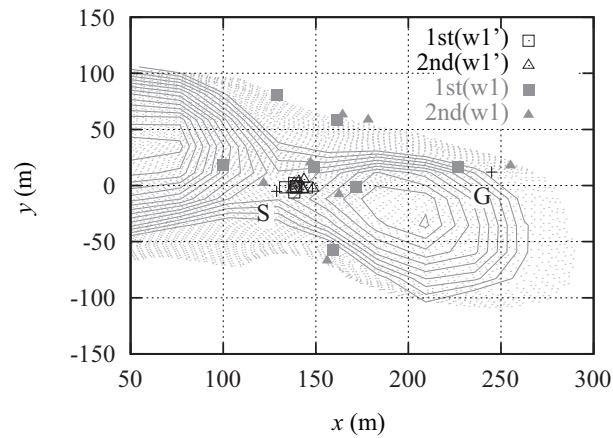
Fig. 5.9: Predicted state from initial action (when preference balance changed to (w1)') : preference balance was changed to (w1'). Predicted state when preferences were slightly changed from (w1) to (w1'). Hopping direction still aimed at goal position, G, however, distance is much smaller, which reduces uncertainties of position of rover.
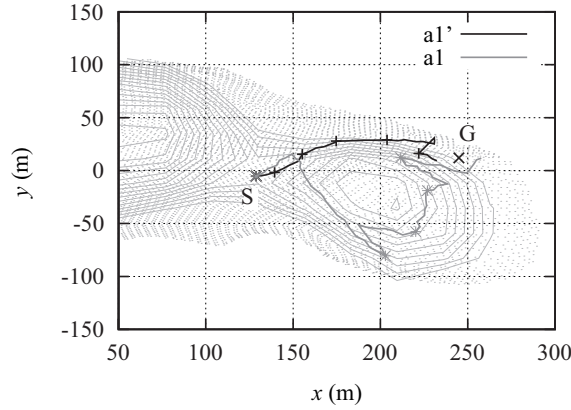
Fig. 5.10: Guidance of a rover with interruption by an operator starting with preference balance (w1): (a1') and (a1) represent trajectories of a rover with and without interruptions by operator, respectively. (a1') prefers smaller hopping motion than (a1) reflecting preference change from (w1) to (w1') which succeeded in reducing total path length as a result.
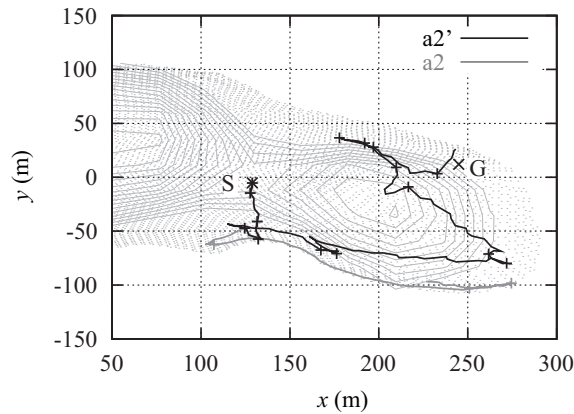

Fig. 5.11: Guidance of a rover with interruption by an operator starting with preference balance (w2): (a2') and (a2) represent trajectories of a rover with and without interruptions by operator, respectively. (a2') was the same trajectories with (a2) in beginning, however, preferences turned from (w2) to (w2') in middle stage of guidance and succeeded in guiding rover to goal position, G.

Chapter 6

Conclusion

In this paper, a rover on a small planetary body has been focused on and a method to localize the rover by a simple device has been proposed. A method to guide a hopping robot, that is, a mobile robot with large uncertainties in locomotion, has been proposed.

A method of localization for a micro robot on small planetary bodies has been proposed, which uses measurements of round-trip propagation delay of radio-waves. The mother spacecraft is used as a single source of radio-waves. The proposed method is similar to GPS [27] in the point that it uses propagation delay of radio waves, though, the proposed method measures the distance between the rover and the mother spacecraft repeatedly to make pseudo-multiple reference points by a single source of radio-waves. The method is able to 1) provide absolute positions of the rover in the planet-centered inertial frame, 2) cover the whole surface of the target planetary body, and 3) be applicable for any size of a planetary body, only requiring a transponder on the rover. Moreover, no synchronization of clocks is needed and no accurate clock is needed on the rover because the proposed method uses the measurements of round-trip propagation delay. The proposed method can be applied to rovers on any size of planetary bodies, while the conventional methods of localization cannot be applied to the rovers on small planetary bodies of less than 1000 m in diameter.

Firstly, the proposed method has been formulated as a recursive method by applying Kalman filter. The calculation of the measurement is non-linear requires two steps of calculation; down-ward and up-ward propagation delay. Each calculation requires to solve equations numerically, and one of them requires to solve simultaneous equations of Kepler's orbit. A method to use the actual position of the mother spacecraft instead of using the estimated position has been proposed, which reduces the amount of computation in measurement into less than half. The simulation results proved that this method to reduce the calculation amount provides as accurate localization as the original method. Secondly, the method of localization has been expanded to a method, which estimates the rotational parameters of the small planetary bodies together with the position of the

rover. The expanded problem includes complex nonlinear and dynamical issues that it cannot be solved analytically. So, the estimation problem has been formulated as an optimization problem to minimize the loss function defined based on the estimation errors derived in comparison with actual measurement data. This optimization problem has been solved by following the gradient vector of the loss function, where the minimum-search based on the gradient had to be divided into three steps. Simulation results proved that the solution based on the variation method is able to estimate both the positions of the rover and the rotational parameters with reasonable accuracy. Thirdly, a method for accurate localization of a space rover on a small planetary body without requiring calculation of differentials has been derived, which can be applied even if the system model contains numerical or empirical formula. The method for the optimization was based on Powell's conjugate direction method [39] and it requires a larger amount of calculations since several forward calculations of the state vector are required for a minimum search [39]. An idea to selectively use the measurement data has been proposed to reduce the computational amount so that the selected data conserves the sensitivity directions. Simple experiments using a range measurement tool validated the estimation convergence and the estimation accuracy of the proposed method of localization.

A model to guide a mobile robot with large uncertainties in locomotion has been proposed. In the proposed model, the decision making of the operator has been modeled as a multi-criteria optimization problem and the preferences of the operator are shared with the robot so that the autonomous action-plan reflects the operator's intuition. In order to provide appropriate interruptions to cope with uncertainties, the probabilistic representation is used for the state prediction of the robot in the proposed model. The proposed model was applied to a guidance problem of a hopping rover on a small planetary body. The application results have proved that the proposed model is effective to guide a hopping rover with ambiguities in hop directions.

Bibliography

[1] R.W. Farquhar, D.W. Dunham, and J.V. McAdams. : NEAR Mission Overview and Trajectory Design. *Journal of Astronautical Sciences*, Vol.43(4), 1995.

[2] J.Kawaguchi, A.Fujiwara, and T.Hashimoto. MUSESC(HAYABUSA): The mission and results. *Proceedings of the IEICE General Conference*, (BK-2-1), 2006.

[3] J.Saito et al. Detailed images of Asteroid 25143 Itokawa from Hayabusa. *Science*, (312):pp. 1341–1344, 2006.

[4] T. Mukai, A.M. Nakamura, and T. Sakai. Asteroidal surface studies by laboratory light scattering and LIDAR on HAYABUSA. *Advances in Space Research*, 37(1), pp.1075-1087, 2006.

[5] T.Yoshimitsu. Autonomous Navigation and Observation on Asteroid Surface by Hopping Rover MINERVA. *Proc. International Symposium on Artificial Intelligence, Robotics and Automation in Space*, 2001.

[6] T. Yoshimitsu, T. Kubota, I. Nakatani, T. Adachi, and H. Saito. Micro-hopping robot for asteroid exploration. *Acta Astronautica*, 52(2-6), pp.441-446, 2003.

[7] http://www.jaxa.jp/article/special/hayabusa/yoshimitsu_e.html.

[8] S.F. Morea. The Lunar Roving Vehicle: A Historical Perspective. *Lunar and Planetary Institute*, 52(2-6), 1988.

[9] R.G. Simmons, S.Thrun, C.Athanassiou, J.Chengand L.Chrisman, R.Goodwin, G.-T.Hsu, and H.Wan. Odysseus: An autonomous mobile robot. *AI Magazine extended abstract*, 1992.

[10] J.J. et al Biesiadecki. Mars exploration rover surface operations: driving opportunity at Meridiani Planum. *Robotics and Automation Magazine, IEEE*, 13(2), pp.63-71, 2006.

[11] Robert Grover Brown and Patrick Y. C. Hwang. *Introduction to Random Signals and Applied Kalman Filtering: With Matlab Exercises and Solutions.* John Wiley & Sons Inc, 1996.

[12] Ernst D. Dicmanns. Vision for ground vehicles: history and prospects. *International Journal of Vehicle Autonomous Systems*, 1(1), pp.1-44, 2003.

[13] F. Lu and E.Milios. Robot pose estimation in unknown environemnts by matching 2d range scans. *Journal of Intelligent and Robotic Systems*, 18(3), 1997.

[14] T.Kubota, K.G.Moesl, and I.Nakatani. Map Matching Scheme for Position Estimation of Planetary Explorer in Natural Terrain. *Proc. IEEE International Conference on Robotics and Automation*, pp.3520-3525, 2007.

[15] D.B.Gennery. Visual terrain matching for a Mars rover. *Proc. IEEE Computer Society Conference on Computer Vision and Pattern Recognition*, pp. 483-491, 1989.

[16] R. Li, F. Ma, F. Xu, L.H. Matthies, C.F. Olson, and R.E. Arvidson. Localization of Mars rovers using descent and surface-based image data. *Journal of Geophysical Research-Planet, FIDO Special Issue*, 107(0):E11, 2002.

[17] F.Cozman and E.Krotkov. Position estimation from outdoor visual landmarks for teleoperation of lunar rovers. *Proc. of the 3rd IEEE Workshop on Applications of Computer Vision*, pages pp.156–161, 1996.

[18] M. Yoshikawa, A. Fujiwara, and J. Kawaguchi. Hayabusa and its adventure around the tiny asteroid Itokawa. *Highlights of Astronomy*, 14, pp.323-324, 2007.

[19] E.W.Yan So, T.Yoshimitsu, and T.Kubota. Relative Localization of a Hopping Rover on an Asteroid Surface using Optical Flow. *Proc. of SICE Annual Conference*, pp.1727-1732, 2008.

[20] S Thrun. *Robotic mapping : A survey. Exploring Artificial Intelligence in the New Millenium.* MorganKaufmann, 2002.

[21] James R. Wertz. *Spacecraft Attitude Determination and Control.* Kluwer Academic Pub, 1978.

[22] C. Pingyuan, Y. Fuzhan, and C. Hutao. Attitude and position determination scheme of lunar rovers basing on the celestial vectors observation. *Proc. of Integration Technology of IEEE International Conference*, pp. 538-543, 2007.

[23] David H. Titterton. *Strapdown Inertial Navigation Technology.* Peter Peregrinus Ltd, 2005.

[24] Mohinder S. Grewal, Lawrence Randolph Weill, and Angus P. Andrews. *Global Positioning Systems, Inertial Navigation, and Integration.* Wiley-Interscience, 2000.

[25] P.C.Thomas. Gravity, Tides, and Topography on Small Satellites and Asteroids: Application to Surface Features of the Martian Satellites. *ICARUS*, 105(2), pp.326-344, 1993.

[26] R.Li, K.Di, L.H. Matthies, R.E.Arvidson, W.M.Folkner, and B.A.Archinal. Rover Localization and Landing-Site Mapping Technology for the 2003 Mars Exploration Rover Mission. *Photogrammetric Engineering & Remote Sensing*, 70(1), pp. 70-90, 2004.

[27] Guochang Xu. *GPS : Theory, Algorithms and Applications.* Springer-Verlag, 2003.

[28] S. Abe et al. Mass and local topography measurements of Itokawa by Hayabusa. *Science*, 312(5778), pp.1344-1347, 2006.

[29] H. Demura et al. Pole and global shape of (25143) Itokawa. *Science*, 312(5778), pp.1347-1349, 2006.

[30] J. K. Miller et.al. Determination of Shape, Gravity, and Rotational Stateof Asteroid 433 Eros. *Icarus*, 155(1), pp.3-17, 2002.

[31] Robert Grover Brown and Patrick Y. C. Hwang. *Introduction to Random Signals and Applied Kalman Filtering: With Matlab Exercises and Solutions.* John Wiley & Sons Inc, 1996.

[32] Sebastian Thrun, Wolfram Burgard, and Dieter Fox. *Probabilistic Robotics (Intelligent Robotics and Autonomous Agents).* The MIT Press, 2005.

[33] T. Katayama. New Edition of Application Kalman Filter. 2000 (in Japanese). (, , , 2000).

[34] D.J. et al. Scheeres. The Dynamical Environment About Asteroid 25143 Itokawa. *Science*, (312):1347–1349, 2006.

[35] S. Nishihara et al. GROUND-BASED LIGHTCURVE OBSERVATION OF (25143) ITOKAWA, 2001-2004. *Lunar Planet. Sci. Conf*, (XXXVI, abstr., 1833), 2005.

[36] A. Fujiwara et.al. The rubble-pile asteroid Itokawa as observed by Hayabusa. *Science*, 312(5778), pp.1338-1341, 2006.

[37] Elijah Polak. *Optimization Algorithms and Consistent Approximations.* Springer, 1997.

[38] Sakawa Masatoshi. *Optimization of Non-linear System— from single criterion to multi criteria* . Morikita Publication, 1986 (in Japanese). (
  —   , 1986).

[39] M.J.D. Powell. An efficient method for finding the minimum of a function of several variables without calculating derivatives. *The Computer Journal*, 7(2), 1964.

[40] Mark Maimone, Andrew Johnson, Yang Cheng, Reg Willson, and Larry Matthies. *Autonomous Navigation Results from the Mars Exploration Rover (MER) Mission*, volume pp.3-13. Springer, 2006.

[41] Gaskell Itokawa Shape Model. http://hayabusa.sci.isas.jaxa.jp/shape.pl. 2010.

[42] S. J. Julier, J. K. Uhlmann, Durrant-Whyte, and H. F. A new approach for filtering nonlinear systems. *American Control Conference*, pp.1628-1632, 1995.

Publications related to this research

Journals

1. Sayaka KANATA, Hiroaki NAKANISHI, Tetsuo SAWARAGI : Method for Accurate Localization of Space Rover without Calculation of Differentials, American Astronautical Society(AAS) (in submission)

2. Sayaka KANATA, Hiroaki NAKANISHI, Tetsuo SAWARAGI : Estimation Method of Rotation Parameters of a Small Planetary Body and Position of a Rover based on Measurements of Round-trip Propagation Delay, Transactions of the Society of Instrument and Control Engineers（Transactions of SICE）, Vol.46 no.5, pp.296-305, 2010 (in Japanese)

3. Sayaka KANATA, Hiroaki NAKANISHI, Tetsuo SAWARAGI, Tetsuo YOSHIMITSU, Ichiro NAKATANI : Radio Wave Based Localization of a Rover for a Small Planetary Body, Journal of Robotics Society of Japan, Vol.27 No.9, pp1-8, 2009 (in Japanese)

Conference and Workshop Papers

Papers for International Conference

1. Sayaka KANATA, Hiroaki NAKANISHI, Tesuo SAWARAGI : Experimental Studies of Localization Method using Round-Trip Range Measurements, 8th International Symposium on Intelligent Automation and Control, ISIAC, Kobe, Japan, September 2010 (submitted)

2. Sayaka KANATA, Hiroaki NAKANISHI, Tesuo SAWARAGI : Man-Machine System Model for Remote Control in Uncertain Environment, 11th IFAC Symposium on Analysis, Design, and Evaluation of Human-Machine Systems, Valenciennes, France, August, 2010 (submitted)

3. Sayaka KANATA, Hiroaki NAKANISHI, Tetsuo SAWARAGI : Localization of a Space Rover and Estimation of Rotational Parameters without Calculating Derivatives, The 14th IASTED International Conference on Robotics and Applications, RA 2009, 664-044, Cambridge, Massachusetts, USA, November 2009

4. Sayaka KANATA, Hiroaki NAKANISHI, Tetsuo SAWARAGI : Localization of a space rover on a small planetary body with uncertain rotation, The IASTED International Conference on Modelling, Simulation and Identification MSI 2009, 659-123, Beijing, China, October, 2009

5. Sayaka KANATA, Hiroaki NAKANISHI, Tetsuo SAWARAGI : Localization Method of Space Rover using Two-Way Range under Uncertainties in Rotational Parameters, ICROS-SICE International Joint Conference, pp. 5260-5264, Fukuoka, Japan, August 2009

6. Sayaka KANATA, Hiroaki NAKANISHI, Tetsuo SAWARAGI, Tetsuo YOSHIMITSU, and Ichiro NAKATANI : Sensitivity Analysis and Influence Discussion of Estimation Errors in Rotation Parameters in Localization of Rovers on Small Planetary Bodies with Single Source of Radio Waves, The SICE Annual Conference, 736, Tokyo, Japan, August 2008

7. Sayaka KANATA, Hiroaki NAKANISHI, Tetsuo SAWARAGI, Tetsuo YOSHIMITSU, and Ichiro NAKATANI : Radio Wave Based Localization of a Rover for a Small Planetary Body, The 27th IASTED International Conference on Modeling, Identification and Control, 596-036, Innsbruck, Austria, February 2008

8. Tetsuo YOSHIMITSU, Sayaka HIGO[1] and Ichiro NAKATANI : Localization on Small Body Surface by Radio Assistance, Technical report of IEICE SANE, Vol.106, No.1(20060403) pp. 145-150, Xian, China, April 2006

9. Sayaka HIGO[1], Tetsuo YOSHIMITSU and Ichiro NAKATANI : Localization on Small Body Surface by Radio Ranging, 16th AAS/AIAA Space Flight Mechanics Meeting, AAS06-148, Florida US, January 2006

Papers for Conference in Japan

1.

2010   ,

2010   6

---

[1]HIGO is birth name of Sayaka KANATA

2.

  pp.360-365
    2009 11

3.

  2009
    1A2-G07   2009 6

4.   , Marek Makowski,   ,
    ,
  , pp.487-490,   2008 12

5.   ,   ,   ,   ,
    , 26
  , 2H1-02,   2008 11

6.

  2008   2P2-A24   2008 6

7.

  25   , 2I25,   2007 9

8.   [1]
  49   2H04   2005 11

9.   [1]   15
    A-16   2005 7

Research Reports

1. Sayaka KANATA, International Institute for Applied Systems Analysis, IIASA Interim Report, IR-08-023, Man-Machine Control of Space Robots under Uncertainty, 2008

Relevant Publications

Journals

1. Kenichi MISHIMA, Sayaka KANATA, Hiroaki NAKANISHI, Tetsuo SAWARAGI, and Yukio HORIGUCHI : Extraction of Similarities and Differences in Human Behavior using Singular Value Decomposition, The Journal of the Institute of Electronics, Information and Communication Engineers　J. IEICE　, (in Japanese, in submission)

2. Hiroaki NAKANISHI, Sayaka KANATA, Tetsuo SAWARAGI, and Yukio HORIGUCHI : Environment adaptive heading control for an autonomous unmanned helicopter, Transactions of the Society of Instrument and Control Engineers　Transactions of SICE　Vol. 46 no.1　pp. 8-15　2010 (in Japanese)

3. Hiroaki NAKANISHI, Sayaka KANATA, Tetsuo SAWARAGI and Yukio HORIGUCHI : Methods to Estimate Magnetic Delination for an Unmanned Aerial Vehicle, Journal of Robotics and Mechatronics, Vol. 20, No. 4, pp. 541–549, 2008 (in Japanese)

Conferences and Workshop Papers

Papers for International Conference

1. Hiroaki NAKANISHI, Sayaka KANATA, Tetsuo SAWARAGI : Environmental Adaptive Yaw Control for Autonomous Unmanned Helicopter and Bifurcation of Maneuvering in Turning, 8th International Symposium on Intelligent Automation and Control, ISIAC, Kobe, Japan, September 2010 (submitted)

2. Kenichi MISHIMA, Sayaka KANATA, Hiroaki NAKANISHI, Tetsuo SAWARAGI, and Yukio HORIGUCHI : Extraction of Similarities and Differences in Human Behavior using Singular Value Decomposition, 11th IFAC/IFIP/IFORS/IEA Symposium on Analysis, Design, and Evaluation of Human-Machine Systems, Valenciennes, France, August 31 - September 3, 2010 (submitted)

3. Hiroaki NAKANISHI, Sayaka KANATA, Tesuo SAWARAGI, Yukio HORIGUCHI : Estimation of Magnetic Declination Angle using Reduced QUEST for an Unmanned Aerial Vehicle, IEEE-ICIT 2010 - IEEE International Conference on Industrial Technology, VD-008257, Vina del Mar - Valparaiso, Chile, March 2010

Papers for Conference in Japan

1.　　　　　　　　　　　　　　　　　　：
　　　　　　　　　　　　　　　　　　　　　　　　　　　　　　　　2010
　　　　　　　　,　　　　2010　6

2.
　　　　　　　　　　　　　　　　2010　　　　　,　　　　2010　6

3.
　　　　　　　　　　　　　　54
　　　　　　2010　5

4.
　　　　　　　　　　　10　SICE
　　　pp.1973-1976　　　2009　12

5.
　　　　　　　　　　　　　,　52
F1-3　2009　11

6.
　　　　　　　　　　　　　　　　52
　　　H6-4　2009　11

7.　　　,　　　　　,
　,　　　　　　　　　　2009　　　　, 1A2-F05,　　2009
6

8.　　　,　　　　,　　　,　　　　,
　　　　　　　　,　53
　　　, pp.409-410,　　2009　5

9.　　　,　　　　,　　　,　　　　,
　　　　　　　　,　53
　　　, pp.611-612,　　2009　5

10.   ,   ,   ,   , 9   , pp.499-500,   2008   12

11.   ,   ,   ,   ,   2008   , pp.413-418,   2008   11

12.   ,   ,   ,   , 26   , CD-ROM,   2008   9

13.   2008   , 1P1-F17,   , 2008   6

14.   52   , pp.357-358,   2008   5

15.   8   (CD-ROM)   pp. 1115-1116, 2007   12

Awards

1. Sayaka KANATA (Kyoto University), 23th Incentive Award of the Robotics Society of Japan, Radio Wave Based Localization of a Rover for Small Planetary Body, June, 2009.

   <div align="center">

   23

   2009　6

   </div>

2. Hiroaki NAKANISHI, Sayaka KANATA, Tetsuo SAWARAGI and Yukio HORIGUCHI, Prize on Excellent Presentation 2008 in System Integration of The Society of Instrument and Control Engineers, Environment adaptive heading control for an autonomous unmanned helicopter and its Improvement, March 2009.

   <div align="center">

   ，　　　，　　　，　　　　SI
   , 2009　3

   </div>

3. Selected and completed the Young Scientists Summer Program in International Institute for Applied Systems Analysis, August, 2008

4. Sayaka HIGO, Prize on Excellent Master's Thesis in 2006 from University of Tokyo, Radio Based Localization on Small Body Surface, February, 2006.

   <div align="center">

   [1]　　17
   2006　3

   </div>